





# Multi-Level Damage-Aware Graph Learning for Resilient UAV Swarm Networks

Huan Lin , Chenguang Zhu , Lianghui Ding , *Member, IEEE*, Feng Yang 

**Abstract**—Unmanned aerial vehicle (UAV) swarm networks leverage resilient algorithms to address communication network split issues and restore connectivity. However, existing graph learning-based resilient algorithms face over-aggregation and non-convergence problems caused by uneven and sparse topology under massive damage scenarios. To alleviate these problems, we propose a novel Multi-Level Damage-Aware Graph Learning (ML-DAGL) algorithm, which generates recovery trajectories by mining information from destroyed UAVs. We first introduce a Multi-Branch Damage Attention (MBDA) module, which forms a sequence of multi-hop Damage Attentive Graphs (mDAG) with different ranges of receptive fields. Each mDAG links only remaining and damaged nodes to ensure a more even degree distribution for mitigating over-aggregation, and utilizes multi-hop dilation to establish more links for sparse topology enhancement. To resort to the mDAG, we propose a Dilated Graph Convolution Network (DGCN), which generates the optimal recovery trajectories with theoretically proven convergence under massive damage cases. Simulation results show that the proposed algorithm can guarantee the connectivity restoration under large swarm and damage scales, while significantly expediting the recovery time by 75.4% and improving the topology uniformity after recovery.

**Index Terms**—Resilient network, UAV swarm, deep learning, graph convolution network.

## I. INTRODUCTION

TECHNOLOGY of unmanned aerial vehicle (UAV) has developed rapidly in recent years and has been widely applied with the advantages of low cost and high flexibility. Meanwhile, to overcome the limited capability of single UAVs, the UAV swarm composed of hundreds of UAVs has been developed to conduct various complex tasks in open and dangerous environments, such as rescue [1], reconnaissance [2], target attack [3], etc. The UAV swarm usually forms an ad-hoc network for collaboration, where task and control information is transmitted between UAVs through wireless communication links. However, the UAV swarm network (USNET) is susceptible as the UAVs face hostile strikes and external destruction. In the worst case, the damage of multiple

UAVs can divide the USNET into isolated sub-nets and thus cause the communication network split (CNS) issue. Several pro-active resilient mechanisms were proposed to reduce the probability of CNS issues via topology enhancement [4]–[6], yet these strategies can not maintain the connectivity under severe damage scenarios. Therefore, the USNET requires reactive resilient algorithms to restore the connectivity in minimum recovery time.

Resilient algorithms were first studied in wireless sensor networks (WSNs) under static scenarios [7]–[10]. Subsequently, with the advent of mobile WSNs, mobility-based algorithms were developed to restore communication connectivity through node movements [11]–[20], and were later extended for USNETs [21]–[24]. These approaches can be categorized into critical node replacement, central aggregation, and optimal planning algorithms. The first category moves the backup neighboring nodes to replace the position of destroyed critical nodes [11]–[14], yet they suffer from severe cascaded motion problems under multiple destroyed UAVs. The second category aggregates the remaining nodes toward a central meeting point [15]–[17], [21], [22], whereas these algorithms often result in prolonged recovery time, as the time is determined by the node farthest from the meeting point. The third category focuses on minimizing the recovery time by planning optimal recovery trajectories for every remaining node [18]–[20]. Through the optimization of individual recovery paths, the algorithm ensures that each node moves along the most efficient route, reducing overall recovery time.

Among existing optimal planning algorithms, graph-learning-based approaches [23], [24] have achieved state-of-the-art performance by considering the interactions between UAV nodes and leveraging the powerful information aggregation capabilities of Graph Convolution Networks (GCN). However, there are two major challenges in using graph-learning algorithms to address CNS issues. The first is spatial over-aggregation that arises from the uneven topology of the remaining network, where certain nodes become highly clustered. This can lead to some nodes focusing excessively on a few high-degree neighbors while neglecting others, resulting in inefficient recovery trajectories that aggregate around high-degree nodes. The second challenge is non-convergence, which occurs under massive damage scenarios where the network becomes sparse as few links remain within disconnected regions. This sparsity can impede the convergence of graph-based algorithms, as nodes lack sufficient local connectivity to effectively propagate information. Consequently, the recovery process may either fail to converge or take significantly longer, especially in the case of extensive damage.

This paper was supported in part by Shanghai Key Laboratory Funding under Grant STCSM15DZ2270400, and in part by the Program for Professor of Special Appointment (Eastern Scholar) at Shanghai Institutions of Higher Learning. (*Corresponding author: Lianghui Ding.*)

Huan Lin, Chenguang Zhu, and Lianghui Ding are with the Institute of Image Communication and Network Engineering, Department of Electronic Engineering, School of Electronic Information and Electrical Engineering, Shanghai Jiao Tong University, Shanghai 200240, China. Email: lhzt715@sjtu.edu.cn; n1cex9@sjtu.edu.cn; lhding@sjtu.edu.cn.

Feng Yang is with the Institute of Wireless Communication Technologies, Department of Electronic Engineering, School of Electronic Information and Electrical Engineering, Shanghai Jiao Tong University, Shanghai 200240, China. Email: yangfeng@sjtu.edu.cn.

In this paper, we propose a Multi-Level Damage-Aware Graph Learning (ML-DAGL) algorithm to overcome the challenges outlined above. With the help of satellite devices or ground stations, UAV nodes can easily obtain global information and leverage the network topology for local computing. The algorithm generates recovery trajectories from valuable information of destroyed UAVs through two steps. First, the Multi-Branch Damage Attention (MBDA) module generates a series of multi-hop Damage-Attentive Graphs (mDAGs), where each mDAG has different ranges of damage awareness. By selectively linking remaining and damaged nodes, mDAG ensures a more even degree distribution and helps mitigate spatial over-aggregation. The multi-hop dilation of mDAG also addresses sparse topologies by establishing links between distant nodes, improving receptive field enhancement in regions with severe damage. Second, the Dilated Graph Convolution Network (DGCN) utilizes these mDAGs to compute optimal recovery trajectories. By employing the Bipartite Graph Convolution Operation (B-GCO) and the residual connection mechanism, the DGCN can preserve the gradient and guarantee convergence even under fragmented topologies of extensive damage scenarios. Simulation results indicate that the proposed algorithm guarantees connectivity restoration across varying damage scenarios, significantly reduces average recovery time, and enhances the recovered topology with a more uniform degree distribution. Our contributions in this paper are summarized as follows.

- 1) We propose a novel ML-DAGL algorithm to address the CNS issue in the USNETs. The damage-attentive information can guide the remaining UAVs to fill up the damaged regions to mitigate over-aggregation, and the multi-hop dilation on damage awareness can establish more links to address the problem of sparse topologies.
- 2) To adapt to diverse damage cases with varying scales, we propose the MBDA module to form numerical mDAGs with different ranges of damage awareness via parallel dilation branches. This module provides multi-level receptive fields for incorporating both local and global network information.
- 3) To ensure connectivity restoration on sparse topology, we propose DGCN that utilizes the mDAGs to compute optimal recovery trajectories with theoretically proved convergence. This achieves more efficient and robust graph learning compared with using the original GCO in [25].
- 4) The proposed algorithm only needs 6.02 Mb parameters and 513 MiB running memory, which is feasible for deployment on practical UAVs. Moreover, the algorithm achieves state-of-the-art resilience based on global information, providing a reference baseline for research on the local-information guided recovery methods.

The remainder of this paper is organized as follows. Section II analyzes the related work. Section III forms the system model of the USNET graph and CNS issue. Section IV describes the specific details of the proposed algorithm, and experiment results are given in Section V. Finally, Section VI presents the conclusion.

## II. RELATED WORK

Resilient recovery algorithms for USNET have become a critical area of research, particularly in scenarios where connectivity is disrupted due to massive node destruction in hostile environments [26]. Various strategies have been developed to address the CNS challenges, focusing on reconnecting divided sub-nets within minimum recovery time. Considering the different motivations for moving the surviving nodes, we can divide the existing mobility-based approaches into critical node replacement, central aggregation, and optimal planning algorithms.

The critical-node replacement algorithms aim to rebuild connectivity by replacing the locations of destroyed critical nodes with the backup neighboring nodes. For example, algorithms in [11], [12] identified the global cut-vertex nodes as the critical nodes and addressed the CNS issues in small networks. Zhang *et al.* [13] extended the recovery algorithm to large-scale WSNs by employing a finite state machine, effectively reducing the complexity of identifying cut-vertex nodes. Younis *et al.* [14] considered a clustered USNET and designated the master nodes as the critical nodes, eliminating the need for additional identification processes. However, the cascaded motion problem under massive damage will increase the moving distances of node replacement and reduce the network's coverage ability [27]. Therefore, the node-replacement algorithms show poor performance in addressing CNS issues under massive damage scenarios.

The central aggregation algorithms guide the remaining nodes towards a pre-defined meeting point, which can ensure the restoration of connectivity. These algorithms have been widely applied in mobile WSNs [15]–[17]. In the field of USNETs, Mi *et al.* [21] proposed to define multiple meeting points, which reduces the average moving distance of edge nodes. Chen *et al.* [22] developed a swarm intelligence-based damage-resilient mechanism that calculates the recovery path for each sub-network as an entire part. This approach allows the network to restore connectivity without losing its original links and achieves path tracking with low communication overhead. However, because all UAVs aggregate towards a single meeting point, the network's recovery time is determined by the node farthest from the meeting point. Consequently, central aggregation methods typically result in longer recovery time costs compared to the other two categories of algorithms.

The optimal-planning algorithms formulate the recovery issues as an optimization problem to minimize the recovery time via planning optimal recovery paths for the remaining nodes [18]–[20]. With the development of UAV intelligence, more advanced approaches integrate deep learning and graph-based algorithms to evolve the network topologies. Mou *et al.* [23] applied the graph convolution network (GCN) to solve the CNS challenge for the first time, where the information aggregation capability of graph learning enables the algorithm to achieve excellent performance on shorter recovery time. Our previous work [24] developed a damage-embedding module that maps the location information of destroyed nodes into the features of their remaining neighbors. This mechanism strengthens the GCN's capability of modeling and reasoning,

improving the performance by inputting more adequate information. However, the uneven topology of the remaining network led to a serious over-aggregation problem as the nodes were attracted to their high-degree neighbors, and the sparse topology after severe damage ultimately degraded the performance of graph learning.

This paper aims to explore a more efficient graph-learning algorithm to eliminate the problems mentioned above. By re-attracting the attention of the remaining nodes to damaged nodes with topology processing, we consider forming a graph with only links between remaining and damaged nodes to avoid the uneven topology and utilizing multi-hop dilation to enhance the sparse topology, thereby achieving fast connectivity restoration and more robust recovered networks.

### III. SYSTEM MODEL

This section first constructs a graph topology to represent the UAV swarm network (USNET) and then proposes the massive damage model. The problem investigated in this paper is formulated in the third subsection.

#### A. UAV Communication Model

Assuming that the USNET is composed of  $N$  massive independent and identical UAVs with a pre-defined connected structure, where the UAVs are labeled by a global index  $\mathcal{I} = \{1, 2, \dots, N\}$ . Generally, UAVs form a network at equal altitudes for most missions, hence we mainly consider two-dimensional locations. The location vector  $\mathbf{p}_i(t) = [x_i(t), y_i(t)]^\top \in \mathbb{R}^2$  denotes the coordinates of the  $i$ -th UAV at time  $t$ , where  $x_i(t)$  and  $y_i(t)$  denote the coordinate component of  $X$  and  $Y$  axis, respectively.

Since we focus on the CNS issue in USNETs, the transmission delay of the air-to-air communication channel is not considered in this paper. Without loss of generality, we consider a predominantly line-of-sight communication link between UAVs in the air. According to Friis transmission formula, the received signal power of  $u_j$  from  $u_i$  is given by

$$P_{ij} = P_0 G_{tx} G_{rx} L(d_{ij}) |h_0|^2, \quad (1)$$

where  $P_0$  is the transmitting power,  $G_{tx}, G_{rx}$  are the constant gains of the transmitting and receiving antennas, respectively. The  $L(d_{ij}) = (\lambda_c/4\pi d_{ij})^2$  is the large-scale fading, where  $\lambda_c$  is the wavelength,  $d_{ij} = \|\mathbf{p}_i - \mathbf{p}_j\|$  is the Eulerian distance between the UAV  $u_i$  and  $u_j$ . The  $|h_0|^2$  is the small-scale fading that follows the Gamma distribution. Denoting the receiver sensitivity  $\tau$ , we can calculate the maximum communication range from the following condition

$$P_0 G_{tx} G_{rx} L(d_{tr}) |h_0|^2 = \tau, \quad (2)$$

and  $u_i$  and  $u_j$  can establish a communication link at time  $t$  when the distance is shorter than the UAV transmission range  $d_{tr}$ , i.e., the edge  $e_{ij} \in \mathcal{E}(t)$  exists if and only if  $d_{ij}(t) \leq d_{tr}$ .

#### B. Graph Topology of USNET

Let graph  $\mathcal{G}(t) = \{\mathcal{U}(t), \mathcal{E}(t)\}$  denote the topology of the USNET, where  $\mathcal{U}(t) = \{u_i | i \in \mathcal{I}(t)\}$  represents the node set and  $\mathcal{E}(t) = \{e_{ij} | u_i, u_j \in \mathcal{U}(t)\}$  represents the edge set of communication links. The edge  $e_{ij}$  exists if and only if node  $u_i$  and  $u_j$  form a communication link. Generally, the USNET establishes an ad hoc network to enable message exchange across the multi-hop links. Denote  $H_{ij}(t)$  as the number of hops between nodes  $u_i$  and  $u_j$  at time  $t$ , which is calculated as the minimum number of transmissions to reach each other. In this case, node  $u_j$  is called a  $k$ -hop neighbor of  $u_i$  at time  $t$  if  $H_{ij}(t) = k$ .

The massive damage can occur at any time and destroy a certain number of UAVs. To simplify the damage model, we determine the moment  $t_0$  that the communication network split (CNS) issue happens, where a total of  $N_D$  UAVs were destroyed and  $N_R = N - N_D$  UAVs remained. The damage index  $\mathcal{I}_D = \{d_1, d_2, \dots, d_{N_D}\}$  labeled all destructed UAVs, and the remain index  $\mathcal{I}_R = \{r_i | r_i \in \mathcal{I} - \mathcal{I}_D\}$  contained the remaining UAV nodes. To model the topology after the damage, we constructed a remaining graph  $\mathcal{G}_R(t) = \{\mathcal{U}_R(t), \mathcal{E}_R(t)\}$  at time  $t \geq t_0$ , where  $\mathcal{U}_R(t) = \{u_{r_i} | r_i \in \mathcal{I}_R\}$  is the remaining-node set, and  $\mathcal{E}_R(t) = \{e_{r_i r_j} | e_{r_i r_j} \in \mathcal{E}(t), r_i, r_j \in \mathcal{I}_R\}$  is the edge set for remaining UAVs.

In this paper, we assume that each UAV periodically reports its position and status information through satellite communication devices. Therefore, the satellite can sense the damaged UAVs and then broadcast the global information, including the damage index and position matrix. The position matrix consisting of the location vectors of each UAV at time  $t$  is defined as

$$\mathbf{X}(t) = [\mathbf{p}_1(t), \mathbf{p}_2(t), \dots, \mathbf{p}_N(t)]^\top \in \mathbb{R}^{N \times 2}. \quad (3)$$

#### C. Network Connectivity

Due to the CNS issue, the remaining graph  $\mathcal{G}_R(t)$  is split into several disconnected sub-nets. Denote  $\mathcal{S}_{all}(t) = \{\mathcal{S}_j(t) | \mathcal{S}_j(t) \subseteq \mathcal{U}_R(t)\}$  as the series of sub-nets in  $\mathcal{G}_R(t)$  at time  $t$ , where sets  $\mathcal{S}_i(t)$  and  $\mathcal{S}_j(t)$  are said to be disconnected at time  $t$  if  $\forall u_k \in \mathcal{S}_i(t)$  can not reach other nodes  $\forall u_l \in \mathcal{S}_j(t)$ .

Let  $N_s(t) = |\mathcal{S}_{all}(t)|$  denote the number of sub-nets in  $\mathcal{G}_R(t)$  at time  $t$ , apparently,  $\mathcal{G}_R(t)$  is connected at time  $t$  if and only if  $N_s(t) = 1$ . A widely-used method to calculate  $N_s(t)$  of  $\mathcal{G}_R(t)$  with the Laplace matrix is introduced in [28]. We first define the adjacency matrix of  $\mathcal{G}(t)$  at time  $t$  as  $\mathbf{A}(t) = (a_{ij}) \in \mathbb{S}^N$ , where  $a_{ij}$  is a 0-1 variable to denote if  $e_{ij}$  exist or not, and  $\mathbb{S}^N$  represents the set of symmetric matrices. Similarly, the adjacency matrix of the  $\mathcal{G}_R(t)$  at time  $t$  is defined as  $\mathbf{A}_R(t) = (a_{r_i r_j}) \in \mathbb{S}^{N_R}$ , and  $a_{r_i r_j} = 1$  if and only if  $e_{r_i r_j} \in \mathcal{E}_R(t)$ . With the adjacency matrix  $\mathbf{A}_R(t)$ , we have the degree matrix of  $\mathcal{G}_R(t)$  as

$$\mathbf{D}_R(t) = \text{diag}(d_{r_1}(t), d_{r_2}(t), \dots, d_{r_{N_R}}(t)), \quad (4)$$

where  $d_{r_i}(t) = \sum_{j=r_1}^{r_{N_R}} a_{r_i r_j}(t)$  is the degree of each remaining node, and  $\text{diag}(\cdot)$  represents a diagonal matrix. The Laplace matrix of  $\mathcal{G}_R(t)$  is define as the difference between  $\mathbf{D}_R(t)$  and  $\mathbf{A}_R(t)$ , i.e.,

$$\mathbf{L}_R(t) = \mathbf{D}_R(t) - \mathbf{A}_R(t). \quad (5)$$

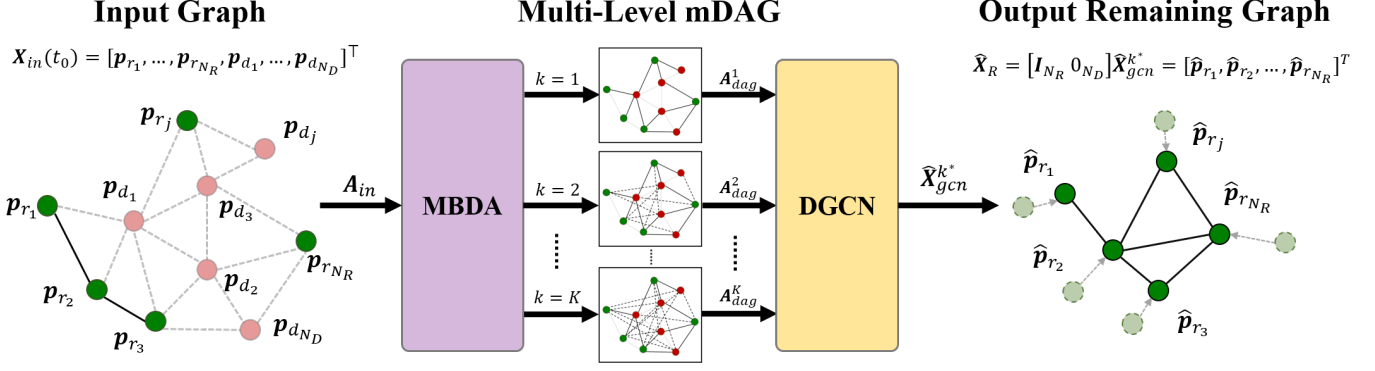


Fig. 1: Overall framework of the proposed ML-DAGL algorithm.

Since the  $\mathbf{L}_R(t)$  is a positive semi-definite matrix, with the eigenvalue decomposition applied on  $\mathbf{L}_R(t)$ , we have

$$\mathbf{L}_R(t) = \mathbf{U}_R(t) \mathbf{\Lambda}_R(t) \mathbf{U}_R^T(t), \quad (6)$$

where  $\mathbf{U}_R(t) = [\mathbf{u}_{r_1}(t), \mathbf{u}_{r_2}(t), \dots, \mathbf{u}_{r_{N_R}}(t)]$  as the unitary matrix composed of orthogonal eigenvectors, and  $\mathbf{\Lambda}_R(t) = \text{diag}(\lambda_{r_1}(t), \lambda_{r_2}(t), \dots, \lambda_{r_{N_R}}(t))$  denotes the matrix with non-negative eigenvalues. The number of sub-net is equal to the number of zero eigenvalues in  $\mathbf{\Lambda}_R(t)$ , i.e.,

$$N_s(t) = \text{Count}(\lambda = 0 | \mathbf{\Lambda}_R(t)). \quad (7)$$

Apparently, for the remaining graph  $\mathcal{G}_R(t_0)$  after the CNS issue, we have  $N_s(t_0) > 1$ .

#### D. Problem Formulation

Mobility-based resilient algorithms aim to restore the connectivity of  $\mathcal{G}_R(t)$  with minimum recovery time via the UAV movement. For the original USNET with  $N$  UAVs, there can be  $2^N$  different damage cases under varying numbers of destroyed UAVs  $N_D$ . Note that not every case will split the network, we only study the damage scenarios in which CNS issues happen at time  $t_0$ . Denote  $T_{r_i}$  as the flying time of the remaining node  $u_{r_i}$  during the recovery process, we have the total recovery time as  $T_{rc} = \max_{r_i \in \mathcal{I}_R} T_{r_i}$ , and the connectivity constraint  $N_S(t_0 + T_{rc}) = 1$  holds.

To find the recovery trajectories of remaining nodes, we need to generate an optimal target position matrix  $\hat{\mathbf{X}}_R = [\hat{\mathbf{p}}_{r_1}, \hat{\mathbf{p}}_{r_2}, \dots, \hat{\mathbf{p}}_{r_{N_R}}]^T$  for the target remaining graph  $\hat{\mathcal{G}}_R$ . The recovery process can be simplified as each node moves towards its target location straightly with its maximum speed  $v_{max}$ . Consequently, the flying time of the remaining node  $u_{r_i}$  from its initial location to the target location is calculated by  $T_{r_i} = \frac{1}{v_{max}} \|\hat{\mathbf{p}}_{r_i} - \mathbf{p}_{r_i}(t_0)\|$ . The total recovery time depends on the maximum time required for the remaining drones to reach their respective target positions. Thus, the problem can be reformulated as

$$(P1): \min_{\hat{\mathbf{X}}_R} T_{rc} = \max_{r_i \in \mathcal{I}_R} \frac{\|\hat{\mathbf{p}}_{r_i} - \mathbf{p}_{r_i}(t_0)\|}{v_{max}} \quad (8)$$

$$\text{s.t. } \hat{N}_S = 1, \quad (9)$$

where  $\hat{N}_S$  is the number of sub-nets in the target remaining graph  $\hat{\mathcal{G}}_R$  recovered by  $\hat{\mathbf{X}}_R$ .

#### IV. APPROACH

This section first introduces the overall framework of the proposed ML-DAGL algorithm. Then, the details of the proposed MBDA module and DGCN are presented in the second and third subsections, respectively. Finally, the proposed algorithm is theoretically analyzed in the last subsection.

##### A. Overall Framework of ML-DAGL

As shown in Fig.1, our proposed ML-DAGL algorithm has an end-to-end architecture that can provide a target position matrix for the remaining graph to solve (P1). The ML-DAGL framework consists of two key components: a Multi-Branch Damage Attention (MBDA) module to form the multi-hop Damage Attentive Graphs (mDAGs), and a Dilated Graph Convolution Network (DGCN) to generate solutions based on mDAGs.

The proposed algorithm first constructs an input graph  $\mathcal{G}_{in}(t_0) = \{\mathcal{U}_{in}, \mathcal{E}_{in}\}$  to resort the index of UAVs based on  $\mathcal{I}_R$  and  $\mathcal{I}_D$ , i.e.,  $\mathcal{I}_{in} = \{r_1, \dots, r_{N_R}, d_1, \dots, d_{N_D}\}$ . Then, we can determine the input feature matrix as the position matrix of  $\mathcal{G}_{in}$ , that is

$$\mathbf{X}_{in}(t_0) = [\mathbf{p}_{r_1}(t_0), \dots, \mathbf{p}_{r_{N_R}}(t_0), \mathbf{p}_{d_1}(t_0), \dots, \mathbf{p}_{d_{N_D}}(t_0)]^T. \quad (10)$$

The adjacent matrix of  $\mathcal{G}_{in}$  is calculated as  $\mathbf{A}_{in} = (a_{in,ij})$  based on  $\mathcal{E}_{in}$ , where  $a_{in,ij} = 1$  if and only if  $u_{in,i}$  and  $u_{in,j}$  form a communication link at time  $t_0$ .

The MBDA module transforms the input adjacent matrix  $\mathbf{A}_{in}$  into several mDAGs via parallel branches. The  $k$ -th branch outputs an mDAG with the adjacent matrix  $\mathbf{A}_{dag}^k$ , which establishes links between remaining and damaged nodes within the range of  $k$ -hop neighbors. With the number of branches  $K$ , the module finally forms  $K$  different mDAGs  $\{\mathbf{A}_{dag}^1, \mathbf{A}_{dag}^2, \dots, \mathbf{A}_{dag}^K\}$ .

The DGCN then outputs an optimal target position matrix  $\hat{\mathbf{X}}_{gcn}^*$ . Consequently, we can determine the optimal target position matrix for (P1) as

$$\hat{\mathbf{X}}_R = [\mathbf{I}_{N_R} \mathbf{0}_{N_D}] \hat{\mathbf{X}}_{gcn}^* = [\hat{\mathbf{p}}_{r_1}^*, \hat{\mathbf{p}}_{r_2}^*, \dots, \hat{\mathbf{p}}_{r_{N_R}}^*]^T, \quad (11)$$

where  $\mathbf{I}_{N_R}$  is the  $N_R$ -by- $N_R$  identity matrix,  $\mathbf{0}_{N_D}$  is the  $N_D$ -by- $N_D$  zero matrix.

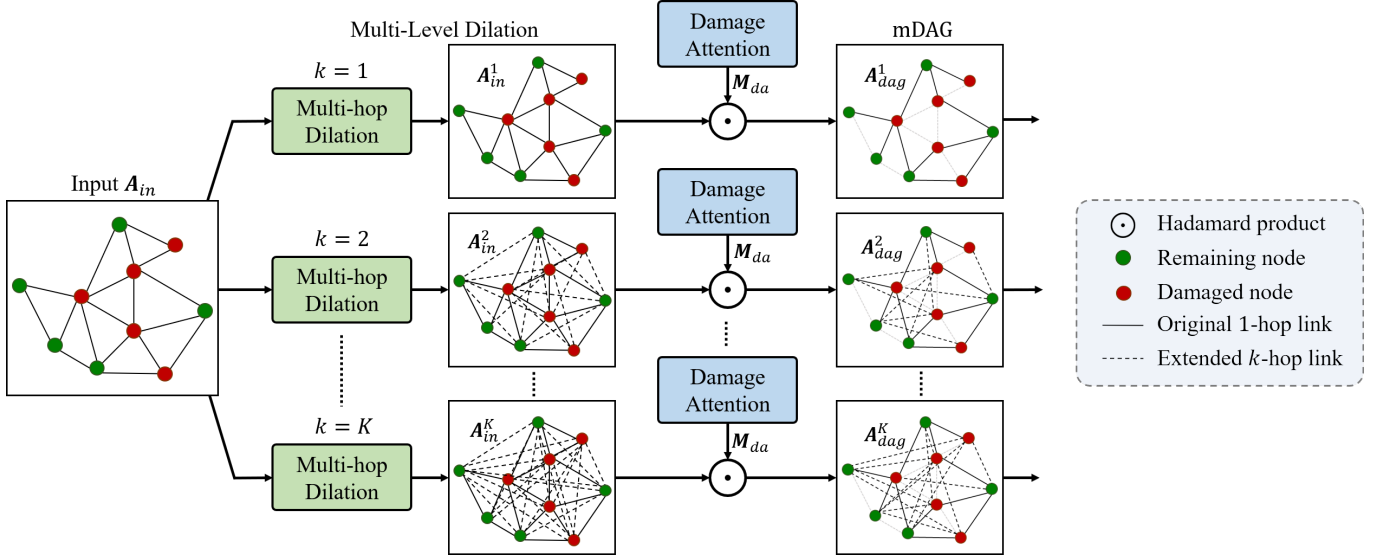


Fig. 2: Structure of the proposed MBDA module.

Notice that the proposed ML-DAGL is an optimization-based resilient algorithm; it requires online iterations to generate an optimal solution for the specific case with distinct input graph  $\mathcal{G}_{in}$ . To reduce the epoch of online iterations, we utilize the pre-trained model to initialize the parameters and skip the warm-up stage in training. Moreover, note that the shape of the input graph  $\mathcal{G}_{in}$  only responds to the number of UAVs  $N$  and parallel branches  $K$ . As a result, the pre-trained model can be adapted to different damage cases under varying  $N_D$ . In summary, the ML-DAGL requires limited online iterations and storage requirements, hence it is feasible for practical deployment on UAVs.

### B. Multi-Branch Damage Attention

The destroyed neighbors of the remaining nodes can effectively depict the damage model within local areas and guide the remaining nodes in filling the gaps in the damaged regions. To achieve this, we propose an MBDA module that extends the receptive fields via multi-hop dilation and applies damage attention to form the mDAG. The module structure is illustrated in Fig.2.

1) *Multi-hop dilation branches*: Graph dilation aims to extend the receptive fields of nodes to their multi-hop neighbors. However, a static dilation size has limited performance when facing dynamic damage scales, since a large dilation size benefits the massive damage scenarios, while small-scale damage only requires a small dilation. In our approach, we develop  $K$  parallel dilation branches to provide mDAG with multi-level damage-aware regions.

As shown in Fig.2, the  $k$ -th branch applies  $k$ -hop dilation on  $A_{in}$  and outputs the dilated adjacent matrix  $A_{in}^k = (a_{in,ij}^k) \in \mathbb{S}^N$ . The element  $a_{in,ij}^k$  is calculated by

$$a_{in,ij}^k = \begin{cases} 1, & H_{in,ij} \leq k; \\ 0, & \text{otherwise,} \end{cases} \quad (12)$$

where  $H_{in,ij}$  denotes the number of hops between nodes  $u_{in,i}$  and  $u_{in,j}$  in  $\mathcal{G}_{in}$ . In other words, with the dilation size as  $k$ ,

the  $A_{in}^k$  will add dilated links between nodes whose number of hops is no larger than  $k$ . After the multi-hop dilation branches, we can get a series of dilated adjacent matrices  $\{A_{in}^1, A_{in}^2, \dots, A_{in}^K\}$ .

2) *Damage attentive graph*: To cope with the over-aggregation problem caused by the uneven topology after damage, we propose the damage attention that focuses on the relations between the remaining nodes and their destroyed neighbors, i.e., only links between the remaining nodes  $u_{r_i}$  and destroyed nodes  $u_{d_j}$  will be kept in the adjacent matrix.

In the proposed MBDA shown in Fig.2, we design a damage attention matrix  $M_{da}$  to transform the adjacent matrix, which is defined as

$$M_{da} = \begin{bmatrix} \mathbf{0}_{N_R} & \mathbf{J}_{N_R, N_D} \\ \mathbf{J}_{N_R, N_D}^\top & \mathbf{0}_{N_D} \end{bmatrix}, \quad (13)$$

where  $\mathbf{J}_{N_R, N_D}$  is a  $N_R$ -by- $N_D$  ones matrix that all elements equal to 1.

The  $k$ -th branch then calculates the adjacent matrix of the mDAG as

$$A_{dag}^k = A_{in}^k \odot M_{da} = \begin{bmatrix} \mathbf{0}_{N_R} & A_{in, r_i d_j}^k \\ A_{in, r_i d_j}^{k\top} & \mathbf{0}_{N_D} \end{bmatrix}, \quad (14)$$

where  $A_{in, r_i d_j}^k$  denotes the  $k$ -hop dilated links between  $u_{r_i}$  and  $u_{d_j}$ , and  $\odot$  denote the Hadamard product operator of matrices. Since the nodes in  $A_{in, r_i d_j}^k$  can be divided into the remaining-node and destroyed-node sets and no links exist between nodes within the same set, the mDAG is so-called a bipartite graph. This property splits the relationships between nodes distributed in uneven sub-nets, ensuring that the remaining nodes in the graph do not interact. After the damage attention processing, we have the mDAG sequence with  $\{A_{dag}^1, A_{dag}^2, \dots, A_{dag}^K\}$ .

The parallel structure of MBDA module eliminates the need to pre-define a static dilation size  $k$ , which allows the algorithm to determine the optimal  $k^*$  for each damage case. While available computational resources constrain the choice of the

number of branches  $K$ , later analysis will demonstrate that the parallel structure significantly reduces both pre-training overhead and storage requirements.

### C. Dilated Graph Convolution Network

Building on the feature matrix  $\mathbf{X}_{in}$  and the mDAG adjacent matrix sequence  $\{\mathbf{A}_{dag}^1, \mathbf{A}_{dag}^2, \dots, \mathbf{A}_{dag}^K\}$  provided by MBDA, we present the structure of DGCN in Fig.3. The backbone of DGCN comprises an input normalization layer, the bipartite GCO layers, the nonlinear activation layers, and an output upscale layer.

1) *Structure of DGCN*: Since each  $\mathbf{A}_{dag}^k$  has a different dilation size  $k$ , we merge these adjacent matrices into a sparse block-diagonal matrix as the input for DGCN, i.e.,

$$\hat{\mathbf{A}}_{dag} = \text{diag}(\mathbf{A}_{dag}^1, \mathbf{A}_{dag}^2, \dots, \mathbf{A}_{dag}^K) \in \mathbb{S}^{KN}. \quad (15)$$

Meanwhile, the feature matrix  $\mathbf{X}_{in}$  is repeated according to the number of dilation branches  $K$  to fit the shape of  $\hat{\mathbf{A}}_{dag}$ , i.e.,

$$\dot{\mathbf{X}}_{in} = \underbrace{[\mathbf{X}_{in}^\top, \mathbf{X}_{in}^\top, \dots, \mathbf{X}_{in}^\top]^\top}_K \in \mathbb{R}^{KN \times 2}. \quad (16)$$

With the repeated feature matrix  $\dot{\mathbf{X}}_{in}$  and the multi-level dilated adjacent matrix  $\hat{\mathbf{A}}_{dag}$  sent into the DGCN backbone, we have the output as

$$\hat{\mathbf{X}}_{gcn} = \text{GCN}(\dot{\mathbf{X}}_{in}, \hat{\mathbf{A}}_{dag}) = [\hat{\mathbf{X}}_{gcn}^{1\top}, \hat{\mathbf{X}}_{gcn}^{2\top}, \dots, \hat{\mathbf{X}}_{gcn}^{K\top}]^\top, \quad (17)$$

where each  $\hat{\mathbf{X}}_{gcn}^k = [\hat{\mathbf{p}}_{r_1}^k, \dots, \hat{\mathbf{p}}_{r_{NR}}^k, \hat{\mathbf{p}}_{d_1}^k, \dots, \hat{\mathbf{p}}_{d_{ND}}^k]^\top \in \mathbb{R}^{N \times 2}$  is a possible solution for (P1). Among these  $K$  possible solutions, we can calculate the recovery time of the  $k$ -th solution as

$$T_{rc}^k = \max_{r_i \in \mathcal{I}_R} \frac{\|\hat{\mathbf{p}}_{r_i}^k - \mathbf{p}_{r_i}(t_0)\|}{v_{max}}. \quad (18)$$

By selecting  $k^* = \arg \min_k T_{rc}^k$ , we can determine the optimal target position matrix as  $\hat{\mathbf{X}}_{gcn}^{k^*}$ .

2) *Bipartite GCO*: Since the  $\hat{\mathbf{A}}_{dag}$  is a block-diagonal matrix, applying GCO on  $\hat{\mathbf{A}}_{dag}$  can be regarded as applying GCO on each  $\mathbf{A}_{dag}^k$ . Due to the special topology of  $\mathbf{A}_{dag}^k$  as a sparse bipartite graph, we design a bipartite GCO (B-GCO) based on the Laplace matrix  $\mathbf{L}_{dag}^k$  of the mDAG according to (4) and (5). The features of the mDAG form a structure in non-Euclidean space, hence the features need to be mapped from the time domain into the frequency domain to achieve the convolution operation. The Fourier transform in the time domain is defined by the eigenvalue decomposition of the Laplace matrix [29], i.e.,

$$\mathbf{L}_{dag}^k = \mathbf{U} \mathbf{\Lambda} \mathbf{U}^\top, \quad (19)$$

where the eigenvalues  $\lambda_j$  denote the frequency and the eigenvectors  $\mathbf{u}_j$  denote the Fourier modes, respectively.

Regarding  $\mathbf{x}$  as a signal in the mDAG, we can define the Fourier transform as  $\tilde{\mathbf{x}} = \text{FT}(\mathbf{x}) = \mathbf{U}^\top \mathbf{x}$  and the inverse Fourier transform as  $\mathbf{x} = \text{IFT}(\tilde{\mathbf{x}}) = \mathbf{U} \tilde{\mathbf{x}}$ . Therefore, the

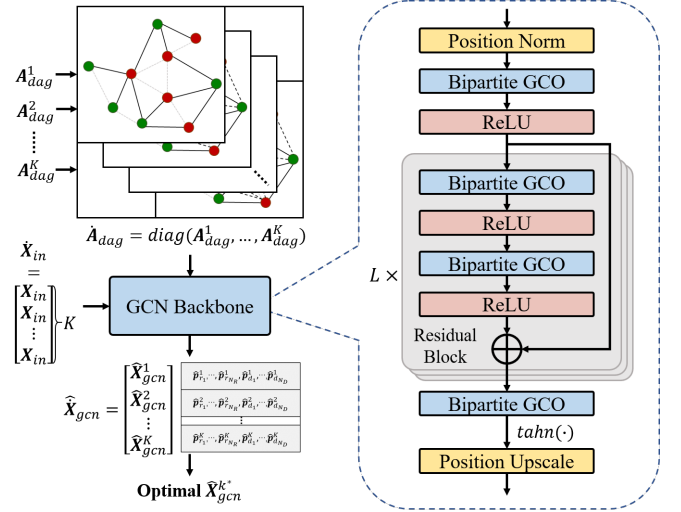


Fig. 3: Structure of the proposed DGCN.

convolution between  $\mathbf{x}$  and the convolution kernel  $g$  can be represented as

$$g * \mathbf{x} = \text{IFT}[\text{FT}(g) \cdot \text{FT}(\mathbf{x})] = \mathbf{U}(\mathbf{U}^\top g \cdot \mathbf{U}^\top \mathbf{x}) \quad (20)$$

where  $*$  is the convolutional operator. Determine  $g$  as a function of  $\mathbf{L}_{dag}^k$ , we can regard  $\mathbf{U}^\top g$  as a function of the eigenvalues  $g_\theta(\mathbf{\Lambda}) = \text{diag}(\theta)$  parameterized by  $\theta \in \mathbb{R}^{|\mathbf{\Lambda}|}$ . Then, the graph convolution is transformed as

$$g_\theta * \mathbf{x} = \mathbf{U} g_\theta \mathbf{U}^\top \mathbf{x}. \quad (21)$$

The complexity of the convolution kernel in (21) can be extremely high since the eigenvalue decomposition requires  $O(n^3)$  computation overhead on global information. A typical approach to decrease the computation complexity is to approximate (21) by truncated Chebyshev polynomials of the first order according to [25], i.e.,

$$\begin{aligned} g_\theta * \mathbf{x} &\approx \mathbf{U} \left( \sum_{c=0}^1 \beta_c T_c(\tilde{\mathbf{\Lambda}}) \right) \mathbf{U}^\top \mathbf{x} = \sum_{c=0}^1 \beta_c T_c(\mathbf{U} \tilde{\mathbf{\Lambda}} \mathbf{U}^\top) \mathbf{x} \\ &= \beta_0 T_0(\tilde{\mathbf{L}}_{dag}^k) \mathbf{x} + \beta_1 T_1(\tilde{\mathbf{L}}_{dag}^k) \mathbf{x} \\ &= \beta_0 \mathbf{x} + \beta_1 (\mathbf{L}_{dag}^k - \mathbf{I}_N) \mathbf{x}, \end{aligned} \quad (22)$$

where  $T_c$  denotes the  $c$ -th item in the Chebyshev polynomials with  $T_0(x) = 1$  and  $T_1(x) = x$ ,  $\beta_c$  is the  $c$ -th Chebyshev coefficient, and  $\tilde{\mathbf{\Lambda}}_d^k = \frac{2}{\lambda_{max}} \mathbf{\Lambda}_d^k - \mathbf{I}_N$  is scaled by the largest eigenvalue of  $\mathbf{L}_d^k$ . Inspired by [23], we define the hyperparameter  $\epsilon = -\beta_1 > 0$  and let  $\beta_0 = \beta_1 + 1$ , then we have the B-GCO of signal  $\mathbf{x}$  in the mDAG as

$$g_\theta * \mathbf{x} = (\mathbf{I}_N - \epsilon \mathbf{L}_{dag}^k) \mathbf{x}. \quad (23)$$

Subsequently, we extend the  $g_\theta$  into a trainable B-GCO layer. In each B-GCO layer, we introduce a weight matrix for feature linear transformation, which serves as the trainable parameter. Specifically, in the  $q$ -th B-GCO layer, the feature matrix is processed by the GCO as

$$\hat{\mathbf{X}}_{gco}^q = \text{GCO}(\hat{\mathbf{X}}_{gco}^{q-1}, \hat{\mathbf{A}}_{dag}) = (\mathbf{I}_{KN} - \epsilon \hat{\mathbf{L}}_{dag}) \hat{\mathbf{X}}_{gco}^{q-1} \mathbf{W}^q, \quad (24)$$

where the Laplace matrix  $\dot{L}_{dag}$  is computed based on  $\dot{A}_{dag}$ , and  $\mathbf{W}^q$  is a layer-specific trainable weight matrix.

3) *DGCN backbone*: As shown in the right part of Fig.3, a position normalization layer takes  $\dot{\mathbf{X}}_{in}$  as input and down-scales the features into the range of  $(-1, 1)$ . Let  $\mathbf{p}_c = \frac{1}{N} \sum_{i=1}^N \mathbf{p}_i(t_0)$  denote the center point of the USNET at time  $t_0$ , hence we can define the scale ratio  $D = \max_{i \in \mathcal{I}} \|\mathbf{p}_c - \mathbf{p}_i(t_0)\|$  is the maximum distance between nodes and  $\mathbf{p}_c$ . The normalized feature matrix as be calculated as

$$\dot{\mathbf{X}}_{norm} = \frac{\dot{\mathbf{X}}_{in} - \mathbf{p}_c^\top}{D + 1}. \quad (25)$$

Next, the normalized feature matrix is sent into a single B-GCO layer, additionally with the ReLU activation function as the non-linear layer. The output feature matrix is

$$\dot{\mathbf{X}}_{gco}^1 = \text{ReLU}\left(\text{GCO}(\dot{\mathbf{X}}_{norm}, \dot{\mathbf{A}}_{dag})\right). \quad (26)$$

Here, the feature dimension is extended from 2 to the hidden dimension  $d_s$  by setting  $\mathbf{W}^1$  as a 2-by- $d_s$  weight matrix.

Subsequently, the output feature matrix is processed by  $L$  residual blocks. Each residual block consists of two B-GCO layers and two ReLU layers, plus a residual connection with  $\dot{\mathbf{X}}_{gco}^1$  at the output. Therefore, the output feature matrix of the  $l$ -th residual block is

$$\dot{\mathbf{X}}_{block}^l = \left[ \text{ReLU}\left(\text{GCO}(\dot{\mathbf{X}}_{block}^{l-1}, \dot{\mathbf{A}}_{dag})\right) \right]^2 + \dot{\mathbf{X}}_{gco}^1. \quad (27)$$

The weight matrices in the residual block are all set as  $d_s$ -by- $d_s$  matrices. Particularly, we have  $\dot{\mathbf{X}}_{gco}^1$  as the input of the first residual block. Note that dropouts [30] can be added between two residual blocks to increase the ability of generalization.

After  $L$  residual blocks, the final B-GCO layer brings the feature dimension back to 2 with the weight matrix set as a  $d_s$ -by-2 matrix. In addition, we introduce a tanh function to map the feature into the range of  $(-1, 1)$ . Therefore, the DGCN has a total of  $Q = 2L + 2$  GCO layers with the output

$$\dot{\mathbf{X}}_{gco}^Q = \tanh\left(\text{GCO}(\dot{\mathbf{X}}_{block}^L, \dot{\mathbf{A}}_{dag})\right). \quad (28)$$

Finally, the output layer up-scales the feature matrix to the target position ranges. The final output position matrix of DGCN is calculated as

$$\hat{\mathbf{X}}_{gcn} = (D + 1) \cdot (\dot{\mathbf{X}}_{gco}^Q + \mathbf{p}_c^\top). \quad (29)$$

4) *Loss function design*: Denote the loss function of the DGCN as  $\mathcal{L}(\dot{\mathbf{X}}_{in}, \mathcal{W})$ , where  $\dot{\mathbf{X}}_{in}$  is the input feature matrix and  $\mathcal{W} = \{\mathbf{W}^1, \mathbf{W}^2, \dots, \mathbf{W}^Q\}$  is the set of layer weight matrices.

Since the output of DGCN  $\hat{\mathbf{X}}_{gcn}$  contains  $K$  possible solutions according to (17), we can calculate a loss for each solution  $\hat{\mathbf{X}}_{gcn}^k$  respectively. To transform the equality constraint (9) as a penalty component in the loss function, we rewrite the problem (P1) as

$$(\text{P1}^\dagger) : \min_{\hat{\mathbf{X}}_{gcn}^k} T_{rc}^k = \max_{r_i \in \mathcal{I}_R} \frac{\|\hat{\mathbf{p}}_{r_i}^k - \mathbf{p}_{r_i}(t_0)\|}{v_{max}} \quad (30)$$

$$\text{s.t. } \hat{N}_S^k - 1 \leq 0, \quad (31)$$

where  $T_{rc}$  is substituted by the recovery time  $T_{rc}^k$  of the solution  $\hat{\mathbf{X}}_{gcn}^k$ , and  $\hat{N}_S^k$  is the number of sub-nets in the remaining graph recovered by  $\hat{\mathbf{X}}_{gcn}^k$ . The equality constraint (9) is represented by the inequality  $\hat{N}_S^k - 1 \leq 0$ . Therefore, we can form a basic loss function of the  $k$ -th solution as

$$\mathcal{L}^k = T_{rc}^k + \lambda(\hat{N}_S^k - 1), \quad (32)$$

where the Lagrange multiplier  $\lambda$  is a positive constant. Based on (32), we define the total training loss of the DGCN as

$$\mathcal{L}_{total} = \sum_{k=1}^K \mathcal{L}^k = \sum_{k=1}^K T_{rc}^k + \lambda(\hat{N}_S^k - 1). \quad (33)$$

#### D. Theoretical Analysis of ML-DAGL

To analyze ML-DAGL, we need to address whether the solution can guarantee connectivity recovery and assess its performance under worst-case scenarios. We first demonstrate that the B-GCO converges for the feature matrix of the mDAG. Subsequently, we derive the theoretical upper bound for the recovery time, relying on the final convergent matrix of the B-GCO.

1) *Convergence of B-GCO*: Since the  $\dot{\mathbf{A}}_{dag}$  is block-diagonal, we can regard the B-GCO on feature matrix  $\dot{\mathbf{X}}_{in}$  as applying B-GCO on  $\mathbf{X}_{in}$  for  $K$  times with different  $\mathbf{A}_{dag}^k$ . For each B-GCO with  $\mathbf{A}_{dag}^k$ , we can prove that it is a contraction operation for each iteration.

*Proposition 1*: In the metric space of position matrices  $\{\mathbf{X}_{gco}\} \subseteq \mathbb{R}^{N \times 2}$ , the B-GCO with  $\mathbf{A}_{dag}^k$  is a contraction operation when  $0 < \epsilon \leq \frac{1}{\|\mathbf{A}_{dag}^k\|_\infty}$ , and there exists and only exists one position matrix  $\bar{\mathbf{X}}_{gco}$  such that

$$\lim_{q \rightarrow \infty} (\mathbf{I}_N - \epsilon \mathbf{L}_{dag}^k)^q \mathbf{X}_{gco} = \bar{\mathbf{X}}_{gco}. \quad (34)$$

Especially, when the B-GCO takes  $\mathbf{X}_{in}$  as the input,  $\bar{\mathbf{X}}_{gco} \equiv [\mathbf{p}_c, \mathbf{p}_c, \dots, \mathbf{p}_c]^\top$  holds when the  $k$ -hop mDAG is connected.

*Proof*: See Appendix A.

Proposition 1 demonstrates that, after a sufficient number of iterations, the B-GCO output  $\hat{\mathbf{X}}_{gco}^k$  converges to  $\bar{\mathbf{X}}_{gco}$ . Since the remaining graph constructed from  $\bar{\mathbf{X}}_{gco} \equiv [\mathbf{p}_c, \mathbf{p}_c, \dots, \mathbf{p}_c]^\top$  is fully connected, we need to find the number of parallel branches  $K$  that ensure at least one connected mDAG with  $k \leq K$ , and determine a proper  $\epsilon$  to meet the convergence constraint for each mDAG with different dilation size  $k$ .

2) *Choice of hyper-parameters*: As the number of nodes  $N$  and the extent of damage  $N_D$  increase, a larger dilation size  $k$  is required to ensure that the mDAG remains connected. However, the number of parallel branches  $K$  limits the maximum value of  $k$  with  $k_{max} = K$ . It can be easily observed that if a  $k$ -hop mDAG with  $\mathbf{A}_{dag}^k$  is connected, then for every  $k_i < k \leq K$ , the  $k_i$ -hop mDAG is connected. Therefore, we only need to ensure that the mDAG is connected in the worst-case scenario. Denote  $H_{max}$  as the maximum hop number in the original USNET, we set the choice of  $K$  as

$$K = \lfloor \frac{H_{max} + 1}{2} \rfloor. \quad (35)$$

where  $\lfloor \cdot \rfloor$  denotes the floor function.

For the choice of  $\epsilon$ , note that  $\|\mathbf{A}_{dag}^k\|_\infty$  is positively correlated to the dilation size  $k$ , but with a limit of  $\|\mathbf{A}_{dag}^k\|_\infty < N$ . To ensure that the convolution kernel  $g_\theta$  remains isomorphic for different  $k$  during the batch process, we set  $\epsilon = \frac{1}{N} < \frac{1}{\|\mathbf{A}_{dag}^k\|_\infty}$  for the bipartite graph convolution to meet the convergence constraint. With the  $K$  in (35), the ML-DAGL algorithm must provide a solution that guarantees connectivity restoration, hence the convergence holds.

3) *Upper bound of recovery time*: Since the final solution  $\hat{\mathbf{X}}_{gcn}^{k*}$  will approach  $\bar{\mathbf{X}}_{gcn}$  when the mDAG is connected, the solution under the worst case refers  $\hat{\mathbf{X}}_R = [\mathbf{p}_c, \dots, \mathbf{p}_c]^\top$  that guarantees the restoration of connectivity. Therefore, we can give an upper bound for the recovery time as

$$T_{rc}^{max} = \sup\{T_{rc}^{k*}\} = \frac{\max_{r_j \in \mathcal{I}_R} \|\mathbf{p}_c - \mathbf{p}_{r_j}(t_0)\|}{v_{max}}. \quad (36)$$

In practical applications, the model often does not need to iterate to  $\bar{\mathbf{X}}_{gco}$  to find a suitable solution, making early termination essential. According to Appendix A, when the number of iterations  $q$  is small, the location of each remaining UAV tends to aggregate around the local damaged region. This characteristic contributes to the performance advantage of the ML-DAGL algorithm.

### E. Computational complexity analysis

The computational complexity of the proposed ML-DAGL consists of the complexities of both MBDA module and DGCN. Since the structure of the ML-DAGL has  $K$  dilation branches, we first analyze the computational complexity of the 1-hop branch, and then generalize it to the  $k$ -hop branch.

1) *Complexity of MBDA*: The matrix operation in MBDA module is the Hadamard product in (14). Since the  $\mathbf{A}_{in}^k$  and  $\mathbf{M}_{da}$  are sparse, the computational complexity of the  $k$ -hop branch is determined as  $\mathcal{O}(\text{nnz}(\mathbf{A}_{in}^k) \cdot \text{nnz}(\mathbf{M}_{da}))$ , where  $\text{nnz}(\cdot)$  is the number of non-zero elements in a matrix. Assuming that  $N$  nodes are randomly distributed within a  $D \times D$  square area, the node degree follows a Poisson distribution. For the 1-hop branch, the number of non-zero elements in  $\mathbf{A}_{in}^1$  can be calculated as

$$\text{nnz}(\mathbf{A}_{in}^1) = \bar{d}N = \pi d_{tr}^2 \rho N, \quad (37)$$

where  $\bar{d}$  is the average node degree,  $d_{tr}$  is the maximum communication range determined by (2),  $\rho = N/D^2$  is the node density. Meanwhile, we have

$$\text{nnz}(\mathbf{M}_{da}) = 2N_D N_R = 2p(1-p)N^2, \quad (38)$$

where  $p = N_D/N$  denotes the damage ratio. Therefore, for the 1-hop branch of the MBDA module, the entire complexity is  $\mathcal{O}(2p(1-p)\bar{d}N^3)$ . For the  $k$ -hop branch, the node degree still follows the Poisson distribution, hence we have  $\text{nnz}(\mathbf{A}_{in}^k) = k\bar{d}N$ . The computational complexity of the MBDA module is finally determined as  $\mathcal{O}(p(1-p)K(K-1)\bar{d}N^3)$ .

In summary, the MBDA module requires a computational complexity of  $\mathcal{O}(K^2 N^3)$ . Since the MBDA module runs only once for each CNS issue, it can be regarded as a data pre-processing stage, and the complexity is acceptable.

2) *Complexity of DGCN*: The matrix operations in DGCN are mainly matrix multiplications in (24).

*Proposition 2*: The computational complexity of the DGCN is given by

$$\mathcal{O}\left(KN \sum_{q=1}^Q [p(1-p)\pi d_{tr}^2 \rho (K-1) + 1 + d_{out}^q] d_{in}^q\right), \quad (39)$$

where  $Q$  is the number of B-GCO layers,  $d_{in}^q, d_{out}^q$  are the input and output dimensions of the  $q$ -th layer.

*Proof*: See Appendix B.

The sparsity of the B-GCO kernel provides the DGCN a linear complexity of  $\mathcal{O}(K^2 N)$  according to Proposition 2. Therefore, the proposed algorithm has computational complexity of  $\mathcal{O}(K^2 N^3 + RK^2 N)$ , where  $R$  is the round of online iterations. For actual practice, the proposed algorithm needs 6.02 Mb parameters and 513 MiB running memory for USNET with 200 UAVs, showing acceptable complexity for practical deployment.

## V. SIMULATION RESULTS

This section first introduces the setup of simulation experiments<sup>1</sup>. Then, comparative results with other advanced approaches are presented in the second subsection, and ablation studies are discussed in the third subsection.

### A. Simulation Setup

1) *Inferences*: The original USNET, consisting of  $N$  UAVs, was randomly distributed within a  $D \times D$  square area, where the node density is set to  $\rho = 200 \text{ node}/\text{km}^2$ . Based on the analysis in [23], we set the communication distance as  $d_{tr} = 120 \text{ m}$ . The maximum value of UAV velocity was defined as  $v_{max} = 10 \text{ m/s}$  for ease of calculation, and each recovery step had a time interval  $\Delta t = 0.1 \text{ s/step}$ . The maximum recovery time is set to  $T_{rc}^{max} = D/2v_{max}$ . The number of destroyed UAVs is given by  $N_D = pN$  according to the damage ratio  $p$ . For the hyperparameter in the proposed algorithm, the number of residual blocks in the DGCN is  $L = 3$ , and the hidden dimension is  $d_s = 512$ . The learning rate is set to 0.0001 with an Adam optimizer, and the dropout ratio is set to 0.1 to alleviate overfitting. The pre-trained model is determined as the parameters after 500 iterations under a random damage case for each  $N$  with  $p = 0.5$ .

2) *Metrics*: Three metrics for performance evaluation were presented in this paper. The *convergent ratio*  $R_c$  represents the proportion of the number of experiments that complete connectivity recovery within  $T_{rc}^{max}$  to the total number of experiments. The higher  $R_c$  indicates a more robust adaptability for different scenarios. The *recovery time*  $T_{rc}$  is the average time for finishing the recovery process to evaluate the performance of different resilient algorithms. Moreover, we introduce *degree distribution*  $P_d$  to measure the topology uniformity of the final recovered  $\hat{\mathcal{G}}_R$ , which denotes the proportion of remaining nodes with a degree number not greater than  $d$  versus the total number of nodes in  $\hat{\mathcal{G}}_R$ . A

<sup>1</sup>The source codes of the proposed ML-DAGL algorithm are available on <https://github.com/lytxzt/Damage-Attentive-Graph-Learning>.

TABLE I: Statistical results of algorithms under half-damaged scenarios with different swarm scales.

Algorithm	$N = 20$				$N = 50$				$N = 100$			
	$R_c$	$E(T_{rc})$	$\sigma(T_{rc})$	$E(d) / \max(d)$	$R_c$	$E(T_{rc})$	$\sigma(T_{rc})$	$E(d) / \max(d)$	$R_c$	$E(T_{rc})$	$\sigma(T_{rc})$	$E(d) / \max(d)$
centering	<b>1.00</b>	1.95	1.35	4.52 / 9	<b>1.00</b>	8.81	6.13	10.25 / 24	<b>1.00</b>	11.02	7.53	11.73 / 49
HERO	0.92	3.93	4.06	4.27 / <b>8</b>	0.26	19.69	9.32	4.45 / <b>11</b>	0.08 <sup>†</sup>	—	—	— / —
SIDR	0.56	8.07	7.11	<b>3.56</b> / <b>8</b>	0.70	9.90	10.11	<b>3.82</b> / <b>11</b>	0.52	25.93	12.02	<b>3.97</b> / <b>11</b>
GCN	<b>1.00</b>	5.09	2.81	5.00 / 9	0.98	12.22	5.00	7.38 / 20	0.90	20.52	9.91	10.73 / 34
GAT	<b>1.00</b>	5.02	3.63	4.88 / 9	<b>1.00</b>	10.28	4.61	7.74 / 20	<b>1.00</b>	14.83	5.70	9.42 / 26
CR-MGC	<b>1.00</b>	2.80	2.59	4.64 / 9	0.98	9.00	5.53	8.44 / 23	<b>1.00</b>	11.14	5.89	9.00 / 30
DEMD	<b>1.00</b>	1.92	1.39	4.49 / 9	<b>1.00</b>	7.78	5.00	8.74 / 23	<b>1.00</b>	10.54	4.91	8.22 / 35
<b>ML-DAGL</b>	<b>1.00</b>	<b>1.74</b>	<b>1.19</b>	3.97 / 9	<b>1.00</b>	<b>3.34</b>	<b>2.38</b>	4.24 / 12	<b>1.00</b>	<b>3.72</b>	<b>1.71</b>	4.53 / <b>11</b>

Algorithm	$N = 200$				$N = 500$				$N = 1000$			
	$R_c$	$E(T_{rc})$	$\sigma(T_{rc})$	$E(d) / \max(d)$	$R_c$	$E(T_{rc})$	$\sigma(T_{rc})$	$E(d) / \max(d)$	$R_c$	$E(T_{rc})$	$\sigma(T_{rc})$	$E(d) / \max(d)$
centering	0.98	22.90	11.17	26.54 / 98	0.88	46.70	18.81	71.04 / 238	0.50	90.12	26.16	260.78 / 463
HERO	0 / —	—	—	— / —	0 / —	—	—	— / —	0 / —	—	—	— / —
SIDR	0.36	34.81	20.43	<b>4.53</b> / 16	0.32	69.94	14.81	<b>4.19</b> / <b>13</b>	0.22	90.64	41.40	<b>4.39</b> / <b>15</b>
GCN	0.86	30.12	12.72	12.14 / 63	0.86	58.52	14.52	56.72 / 214	0.08	—	—	— / —
GAT	<b>1.00</b>	24.48	9.64	13.32 / 65	0.94	56.90	12.98	21.81 / 96	0.80	95.83	13.50	38.12 / 219
CR-MGC	<b>1.00</b>	21.28	8.68	17.66 / 84	0.76	63.84	14.34	29.39 / 108	0.34	104.13	15.62	33.38 / 188
DEMD	<b>1.00</b>	21.40	7.32	13.37 / 53	<b>1.00</b>	45.40	8.72	18.14 / 67	0.68	86.89	22.79	25.77 / 140
<b>ML-DAGL</b>	<b>1.00</b>	<b>5.24</b>	<b>2.10</b>	5.24 / <b>15</b>	<b>1.00</b>	<b>18.10</b>	<b>7.69</b>	7.46 / 30	<b>1.00</b>	<b>32.58</b>	<b>6.18</b>	8.53 / 39

<sup>†</sup>Results with  $R_c < 0.1$  indicate that the algorithm fails to converge in most cases so that other metrics are not statistically significant.

more uniform degree distribution leads to a network that is more robust against attacks [31].

### B. Comparative Results Evaluation

To comprehensively evaluate the performance of our proposed algorithm, we compare it with several advanced resilient approaches, including the traditional algorithms (direct-centering, HERO [21], SIDR [22]) and the graph-learning algorithms (original GCN [25], GAT [32], CR-MGC [23], DEMD [24]).

1) *Scalability on swarm scales  $N$* : To evaluate the scalability of the proposed algorithm for varying swarm scales, we set the number of UAVs as  $N \in \{50, 100, 200, 500, 1000\}$ . The damage ratio is set to  $p = 0.5$ , and each simulation of different  $N$  is repeated 50 times randomly for the statistical results.

Simulation results of the convergent ratio  $R_c$ , mean recovery time  $E(T_{rc})$ , variance of recovery time  $\sigma(T_{rc})$ , average node degree  $E(d)$ , and maximum node degree  $\max(d)$  with different resilient algorithms are presented in TABLE I. For the convergence  $R_c$  of each resilient algorithm, it can be observed that the proposed ML-DAGL can always guarantee the restoration of connectivity under varying scales, while other algorithms have decreasing  $R_c$  and lack the scalability on large swarms, especially when  $N$  reaches 1000. For the recovery time, ML-DAGL achieves state-of-the-art performance on both means

and variances of  $T_{rc}$ , showing an average of 54.9% reduction compared to previous algorithms, and more stable solutions for CNS issues under different  $N$ . In terms of the node degree distribution, SIDR has the lowest  $E(d)$  and  $\max(d)$  owing to its distributed recovery implementation. Over the graph learning-based recovery algorithms, ML-DAGL achieves a lower-degree distribution. This indicates that the proposed algorithm solves the challenge of over-aggregation, significantly improving the topologies of recovered USNETs.

2) *Adaptability on damage scales  $N_D$* : To further explore the adaptability of the proposed algorithm under varying damage scales, we randomly destroy 10 to 190 UAVs with the original USNET set as  $N = 200$ , distributed within a  $1 \text{ km} \times 1 \text{ km}$  area. The maximum recovery time is set to  $T_{rc}^{max} = 50 \text{ s}$ , and similarly, each destruction experiment is repeated 50 times for statistical results.

The convergent ratios of each resilient algorithm are illustrated in Fig.4. The convergence of HERO, SIDR, GCN, and GAT decreases rapidly as the number of destroyed UAVs increases, while the convergent ratios of centering, CR-MGC, and DEMD, remain close to 1 under varying damage scenarios. However, these algorithms cannot guarantee the connectivity when  $N_D$  exceeds 150. For the proposed algorithm, the convergent ratio always equals 1, which demonstrates that all cases of CNS issues are solved. Therefore, the proposed algorithm has better convergence on sparse topologies caused by extremely massive damage.

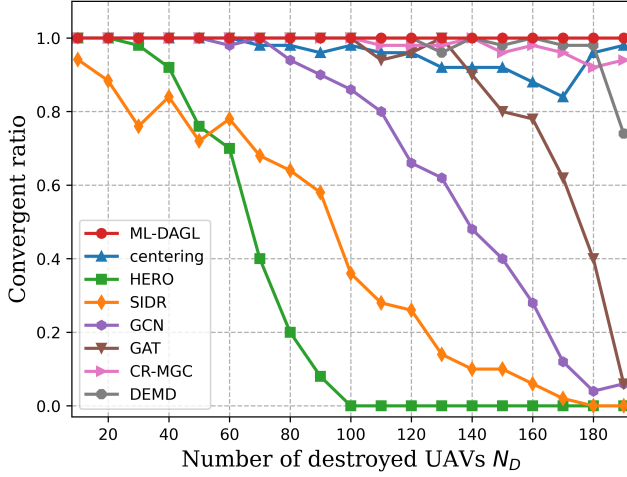


Fig. 4: Results of convergent ratio  $R_c$  under different numbers of destroyed UAVs  $N_D$ .

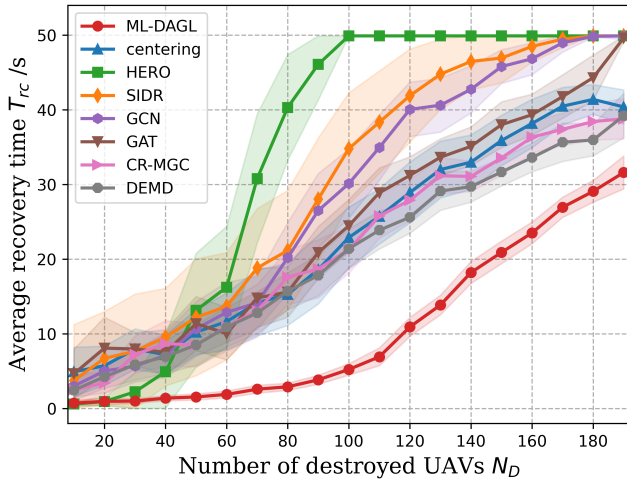
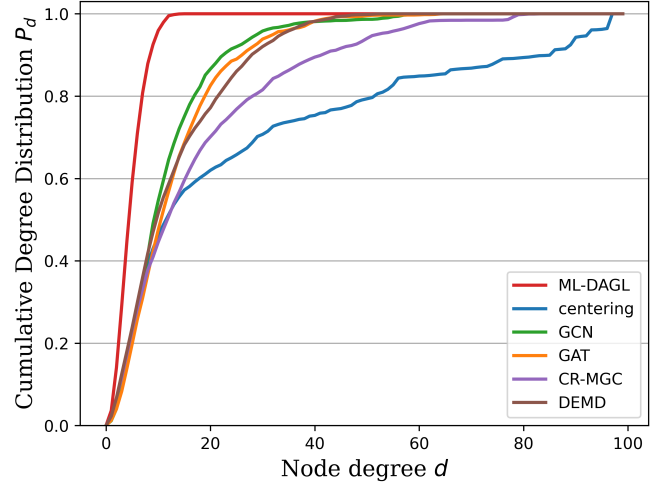


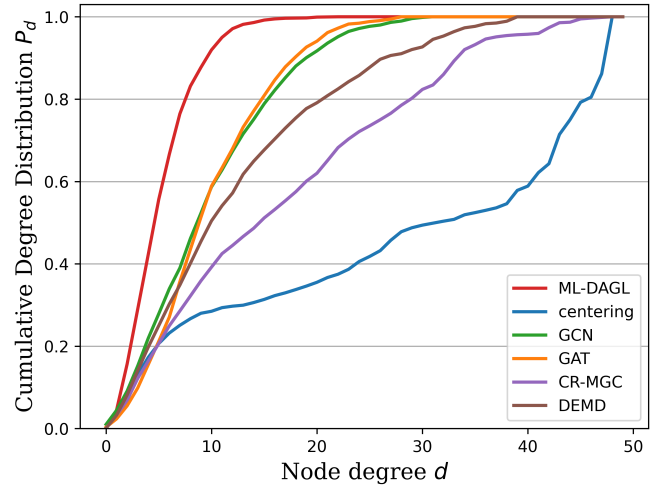
Fig. 5: Results of average recovery time  $T_{rc}$  under different numbers of destroyed UAVs  $N_D$ .

The average recovery time  $T_{rc}$  of different resilient algorithms under damage of different  $N_D$  are shown in Fig.5, where the shaded areas represent the 99% confidence intervals of the average recovery time. We can see that larger damage scales  $N_D$  require longer recovery time across all approaches. Once the damage exceeds 100 nodes, this growth trend accelerates significantly. Referring to the comparative results, the proposed ML-DAGL algorithm shows notable performance improvements in recovery time with an average of 59.8% reduction compared with existing approaches. Specifically, for the half-damaged scenario with  $N_D = 100$ , the average recovery time of the proposed algorithm is cut by 75.4% compared with CR-MGC and DEMD, which is a great margin of 16 seconds. Therefore, the proposed algorithm can accelerate the recovery process of CNS issues under varying damage scenarios.

The cumulative node-degree distributions under 100 and 150 destroyed UAVs with  $N = 200$  are illustrated in Fig.6a and Fig.6b. The results indicate that the degree distributions



(a) cumulative degree distributions under  $N_D = 100$



(b) cumulative degree distributions under  $N_D = 150$

Fig. 6: Results of cumulative degree distribution  $P_d$  under different numbers of destroyed UAVs  $N_D$ .

of the proposed algorithm are primarily concentrated in low-degree regions, with a faster-increasing curve. In contrast, other approaches tend to have higher-degree nodes within the recovered topologies. Therefore, the ML-DAGL helps to rebuild a network with a more sparse and uniform topology after recovery, and the absence of large-degree nodes also improves the swarm resilience when the USNET faces the risk of secondary damage.

3) *Case study*: To compare the performance of different resilient algorithms more intuitively, we introduce a specific example to demonstrate the network recovery process based on each approach. As shown in Fig.7a, we randomly destroy  $N_D = 100$  UAVs of the original USNET, and the remaining graph is divided into 7 disconnected sub-nets with different sizes, leading to an uneven topology. The numbers of sub-nets during the recovery process by different algorithms are illustrated in Fig.7b. It takes only 2.4s for the proposed algorithm to rebuild a connected remaining graph, while other algorithms require much more recovery time. Moreover, the

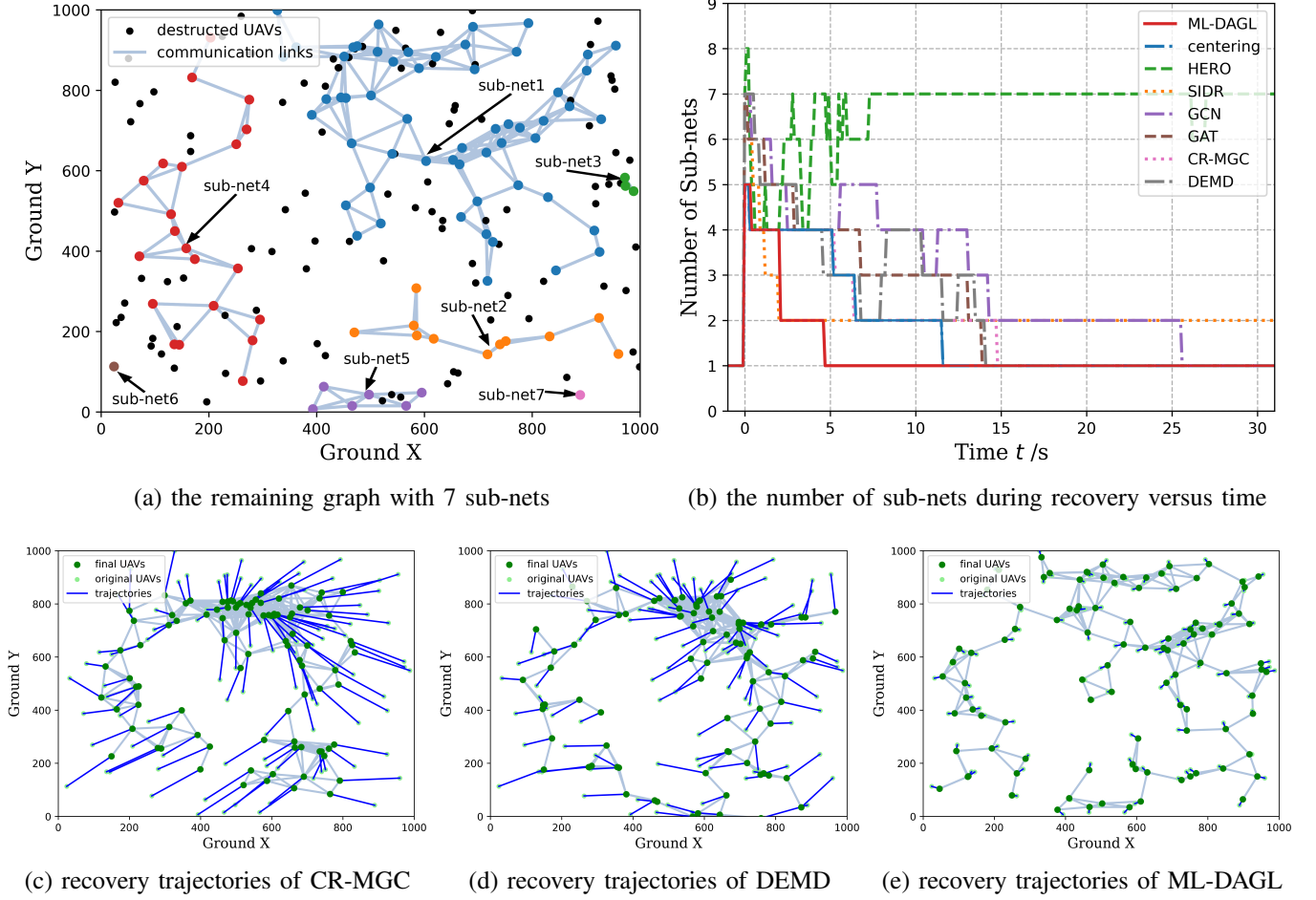


Fig. 7: Results of the case study of different algorithms.

recovery trajectories of CR-MGC, DEMD, and ML-DAGL are plotted respectively. Obviously, the remaining nodes in Fig.7c and Fig.7d tend to aggregate towards sub-net 1 as it is the largest sub-net with the highest degrees, thus causing the over-aggregation problem. The trajectories of ML-DAGL in Fig.7e are quite shorter, and the moving directions of the remaining nodes are towards the damaged regions nearby. Therefore, the proposed algorithm can provide solutions with wider spatial distributions and more uniform topologies, thereby improving communication coverage and alleviating the problem of local over-aggregation.

4) *Response time of algorithms:* The average time consumption of different algorithms is compared in Fig.8. It is worth noting that the centering, HERO, and SIDR require online calculation on every execution step, hence, the entire time consumption of these algorithms is related to their time cost of the recovery process. The graph-learning algorithms only need to calculate the recovery solution when the damage occurs. Compared with other graph-learning approaches, the proposed algorithm has acceptable time consumption for addressing CNS issues. This is because the ML-DAGL requires fewer iterations of GCO thanks to the pre-trained model, which is discussed in a later subsection of the ablation study.

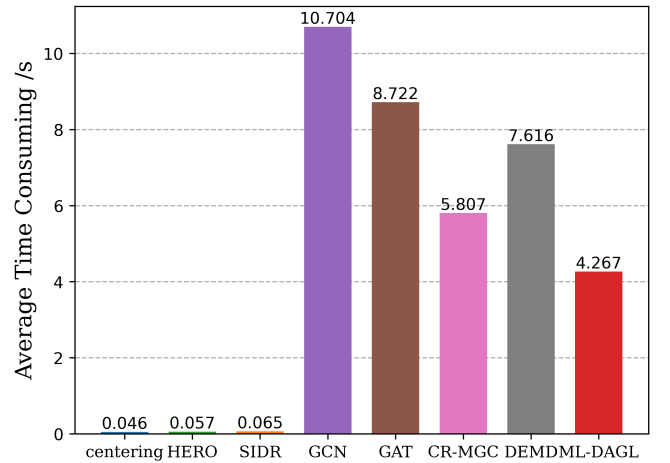


Fig. 8: Results of average time consumption of different algorithms under  $N = 200$ .

### C. Ablation Study

To analyze the effectiveness of each component in the ML-DAGL algorithm framework, we conduct several ablation experiments under the swarm scale set to  $N = 200$ .

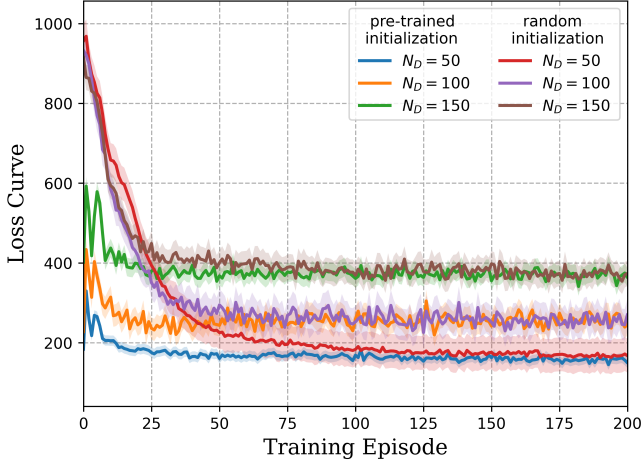


Fig. 9: Loss curve of ML-DAGL training with pre-trained and random initialization under different  $N_D$ .

1) *Study of mDAG sequence*: We first consider the damage-attention in the proposed algorithm. Although the comparative results proved that mDAG can accelerate the recovery process and mitigate the over-aggregation problem, there is still a great advantage of utilizing mDAG sequence as the input of GCN, that is, it uses a unified input matrix framework. Therefore, when the number of UAVs in the original USNET is fixed, only one pre-trained model is necessitated which can adapt to damage scenarios with different  $N_D$ . This significantly reduces storage needs for pre-trained parameters and decreases the overhead of online iterative computing. The loss curves of ML-DAGL during the training process are plotted in Fig.9, where the weights  $W$  in (24) are initialized by pre-trained model and random parameters, respectively. The loss curves initialized by the pre-trained model started from smaller loss values and achieved a smooth stage at the 50th episode. This means that using a pre-trained model can reduce the time consumption for addressing CNS issues. Meanwhile, the same pre-trained model can initialize the ML-DAGL under different  $N_D$  with similar curve trends. Therefore, the proposed algorithm has less storage requirement of only one pre-trained model, while CR-MGC needs 199 meta-learning models.

2) *Study of MBDA*: The proposed MBDA module offers two advantages to ML-DAGL. First, it applies multi-hop dilation to extend the receptive fields of nodes under massive damage scenarios. Second, it has a structure of parallel dilation branches, which allows the parallel computation of solutions  $\hat{X}_{gcn}^k$  with different dilation sizes  $k$ , optimizing the recovery path for varying damage scales. The recovery time of the MBDA with  $k$ -hop and parallel dilation is shown in Fig.10. The results demonstrate that the optimal value of dilation size  $k$  corresponds to the scale of destruction, e.g., the best choice of  $k$  is  $k = 3$  when  $N_D = 100$  while it becomes  $k = 9$  when  $N_D = 150$ . Compared with specific dilation size  $k$ , the parallel dilation has a shorter recovery time across all  $N_D$ . Although the parallel structure increases the number of parameters, the ML-DAGL algorithm has only a 6.02Mb model size that is manageable given the performance gains achieved.

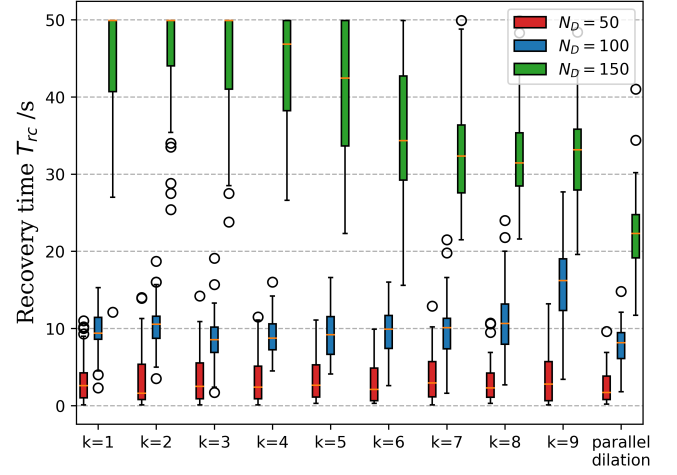


Fig. 10: Average recovery time of MBDA with  $k$ -hop and parallel dilation under different  $N_D$ .

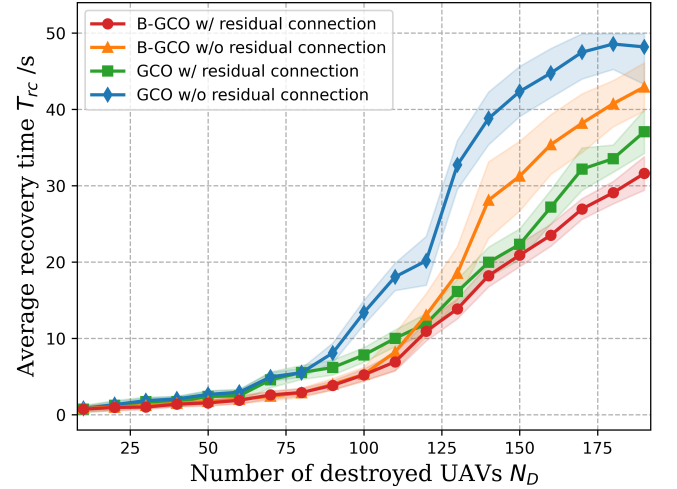


Fig. 11: Average recovery time of DGCN with/without key components under different  $N_D$ .

3) *Study of DGCN*: The proposed DGCN has two key components for generating solutions to CNS issues, i.e., the B-GCO and the residual connection mechanism. The average recovery time of ablation experiments on DGCN is plotted in Fig.11, where the B-GCO is replaced by the original GCO in [25] and the residual connection is optional. The results indicate that DGCN without the residual connection requires a longer recovery time when  $N_D$  gets larger, as the convolution becomes inefficient on a sparse topology. This positively shows the effectiveness of the residual connection under extremely massive damage. Meanwhile, the B-GCO is outperforming the original GCO with an average 22.4% margin. This is because the original GCO normalizes the degree at the node level, while B-GCO uses degree normalization at the graph level, which allows nodes to retain the original degree weight information. As a result, the DGCN can efficiently utilize the original network information to address CNS issues.

## VI. CONCLUSION

In this paper, we study the CNS issue of the USNET under massive damage scenarios. To cope with the challenges of utilizing graph-learning approaches to generate optimal recovery trajectories, we propose a novel ML-DAGL algorithm. To adapt to diverse damage cases with varying scales, we introduce the MBDA module to form a sequence of mDAGs with different ranges of receptive fields. The mDAG links only remaining and damaged nodes to ensure a more even degree distribution for mitigating over-aggregation and utilizes multi-hop dilation to establish more links for sparse topology enhancement. We then develop the DGCN to generate the optimal recovery trajectories based on the mDAG sequence, which can ensure convergence under massive damage cases through B-GCO and residual connection. Statistical results demonstrated that the proposed algorithm can guarantee the connectivity restoration under varying swarm and damage scales, along with significant improvements in both recovery time and topology degree distribution.

### APPENDIX A

#### PROOF OF PROPOSITION 1

In the metric space of position matrices  $\{\mathbf{X}_{gco}\} \subseteq \mathbb{R}^{N \times 2}$ , we can represent the matrix form of B-GCO  $\mathbf{X}_{gco}^{l+1} = g_\theta * \mathbf{X}_{gco}^l = (\mathbf{I}_N - \epsilon \mathbf{L}_{dag}^k) \mathbf{X}_{gco}^l$  as

$$\begin{pmatrix} x_1^{l+1} & y_1^{l+1} \\ x_2^{l+1} & y_2^{l+1} \\ \vdots & \vdots \\ x_N^{l+1} & y_N^{l+1} \end{pmatrix} = \begin{pmatrix} l_{11}^k & l_{12}^k & \dots & l_{1N}^k \\ l_{21}^k & l_{22}^k & \dots & l_{2N}^k \\ \vdots & \vdots & \ddots & \vdots \\ l_{N1}^k & l_{N2}^k & \dots & l_{NN}^k \end{pmatrix} \begin{pmatrix} x_1^l & y_1^l \\ x_2^l & y_2^l \\ \vdots & \vdots \\ x_N^l & y_N^l \end{pmatrix}, \quad (40)$$

where  $x_i$  and  $y_i$  denote the coordinate component of  $X$  and  $Y$  axis from the position vector  $\mathbf{p}_i$  of UAV  $u_i$ , and  $l_{ij}^k$  is the element of  $\mathbf{I}_N - \epsilon \mathbf{L}_{dag}^k$ . Denote  $d_i^k = \sum_{j=1}^N a_{ij}^k$  as the degree of node  $u_i$  from the mDAG, we have

$$\sum_{i=1}^N l_{ij}^k = 1 + \epsilon d_i^k - \epsilon \sum_{j=1}^N a_{ij}^k = 1. \quad (41)$$

The B-GCO can guarantee the invariance of column sums, i.e.,

$$\sum_{i=1}^N x_i^{l+1} = \sum_{i=1}^N \sum_{j=1}^N l_{ij}^k x_j^l = \sum_{j=1}^N (x_j^l \sum_{i=1}^N l_{ij}^k) = \sum_{j=1}^N x_j^l, \quad (42)$$

and the equality  $\sum_{i=1}^N y_i^{l+1} = \sum_{j=1}^N y_j^l$  can be proved in the same manner.

Therefore, the B-GCO is closed for the metric space  $\{\mathbf{X}_{gco} | \sum_{i=1}^N x_i = X_{sum}, \sum_{i=1}^N y_i = Y_{sum}\}$ , which means every position matrix  $\mathbf{X}_{gco}^l$  share a same central location  $\mathbf{p}_c = \frac{1}{N} \sum_{i=1}^N \mathbf{p}_i = [\frac{1}{N} X_{sum}, \frac{1}{N} Y_{sum}]^\top$  from  $\mathbf{X}_{gco}$ .

Then we use the *Contraction Mapping Principle* to prove the B-GCO is a contraction operation and the position matrix  $\mathbf{X}_{gco}$  is convergent to a certain matrix  $\bar{\mathbf{X}}_{gco}$ . We first define the distance between two position matrices  $\mathbf{X}_{gco}^a$  and  $\mathbf{X}_{gco}^b$  as

$$\begin{aligned} d(\mathbf{X}_{gco}^a, \mathbf{X}_{gco}^b) &= \|\mathbf{X}_{gco}^a - \mathbf{X}_{gco}^b\|_\infty \\ &= \max_{1 \leq i \leq N} \{|x_i^a - x_i^b| + |y_i^a - y_i^b|\}. \end{aligned} \quad (43)$$

The distance between the B-GCO of  $\mathbf{X}_{gco}^a$  and  $\mathbf{X}_{gco}^b$  is then calculated as

$$\begin{aligned} d(g_\theta * \mathbf{X}_{gco}^a, g_\theta * \mathbf{X}_{gco}^b) &= \|g_\theta * \mathbf{X}_{gco}^a - g_\theta * \mathbf{X}_{gco}^b\|_\infty \\ &= \|(\mathbf{I}_N - \epsilon \mathbf{L}_{dag}^k)(\mathbf{X}_{gco}^a - \mathbf{X}_{gco}^b)\|_\infty. \end{aligned} \quad (44)$$

Since the infinity norm of matrix  $\|\cdot\|_\infty$  has the sub-multiplicative property, we can get

$$\begin{aligned} d(g_\theta * \mathbf{X}_{gco}^a, g_\theta * \mathbf{X}_{gco}^b) &\leq \|\mathbf{I}_N - \epsilon \mathbf{L}_{dag}^k\|_\infty \|\mathbf{X}_{gco}^a - \mathbf{X}_{gco}^b\|_\infty \\ &= \max_{1 \leq i \leq N} \{1 - \epsilon d_i^k + \sum_{j=1}^N \epsilon a_{ij}^k\} \|\mathbf{X}_{gco}^a - \mathbf{X}_{gco}^b\|_\infty. \end{aligned} \quad (45)$$

Notice that  $d_{ij}^k \leq \|\mathbf{A}_{dag}^k\|_\infty$ , when  $0 < \epsilon \leq \frac{1}{\|\mathbf{A}_{dag}^k\|_\infty}$ , there is

$$1 - \epsilon d_i^k \geq 1 - \epsilon \|\mathbf{A}_{dag}^k\|_\infty \geq 1 - \frac{1}{\|\mathbf{A}_{dag}^k\|_\infty} \|\mathbf{A}_{dag}^k\|_\infty = 0, \quad (46)$$

hence we have

$$\begin{aligned} d(g_\theta * \mathbf{X}_{gco}^a, g_\theta * \mathbf{X}_{gco}^b) &\leq \max_{1 \leq i \leq N} \{1 - \epsilon d_i^k + \sum_{j=1}^N \epsilon a_{ij}^k\} \|\mathbf{X}_{gco}^a - \mathbf{X}_{gco}^b\|_\infty \\ &= \max_{1 \leq i \leq N} \{1 - \epsilon d_i^k + \sum_{j=1}^N \epsilon a_{ij}^k\} \|\mathbf{X}_{gco}^a - \mathbf{X}_{gco}^b\|_\infty \\ &= \max_{1 \leq i \leq N} \{1 - \epsilon \sum_{j=1}^N a_{ij}^k + \sum_{j=1}^N \epsilon a_{ij}^k\} \|\mathbf{X}_{gco}^a - \mathbf{X}_{gco}^b\|_\infty \\ &= \max_{1 \leq i \leq N} \{1\} \|\mathbf{X}_{gco}^a - \mathbf{X}_{gco}^b\|_\infty \\ &= d(\mathbf{X}_{gco}^a, \mathbf{X}_{gco}^b). \end{aligned} \quad (47)$$

The condition for (47) to take the equal sign is

$$\begin{aligned} &\|(\mathbf{I}_N - \epsilon \mathbf{L}_{dag}^k)(\mathbf{X}_{gco}^a - \mathbf{X}_{gco}^b)\|_\infty \\ &= \|\mathbf{I}_N - \epsilon \mathbf{L}_{dag}^k\|_\infty \|\mathbf{X}_{gco}^a - \mathbf{X}_{gco}^b\|_\infty. \end{aligned} \quad (48)$$

Given the proof of the sub-multiplicative property of  $\|\cdot\|_\infty$  as

$$\begin{aligned} &\|(\mathbf{I}_N - \epsilon \mathbf{L}_{dag}^k)(\mathbf{X}_{gco}^a - \mathbf{X}_{gco}^b)\|_\infty \\ &= \max_{1 \leq i \leq N} \{|\sum_{j=1}^N l_{ij}^k (x_j^a - x_j^b)| + |\sum_{j=1}^N l_{ij}^k (y_j^a - y_j^b)|\} \\ &\leq \max_{1 \leq i \leq N} \{\sum_{j=1}^N |l_{ij}^k (x_j^a - x_j^b)| + \sum_{j=1}^N |l_{ij}^k (y_j^a - y_j^b)|\} \\ &= \max_{1 \leq i \leq N} \{\sum_{j=1}^N |l_{ij}^k| \cdot (|x_j^a - x_j^b| + |y_j^a - y_j^b|)\} \\ &\leq \max_{1 \leq i \leq N} \sum_{j=1}^N |l_{ij}^k| \cdot (\max_{1 \leq j \leq N} \{|x_j^a - x_j^b| + |y_j^a - y_j^b|\}) \\ &= \|\mathbf{I}_N - \epsilon \mathbf{L}_{dag}^k\|_\infty \|\mathbf{X}_{gco}^a - \mathbf{X}_{gco}^b\|_\infty. \end{aligned} \quad (49)$$

we can see that inequality (49) is scaled for twice. The first scaling is based on the triangle inequality, hence the condition to take the equal sign is  $l_{ij}^k (x_j^a - x_j^b) \geq 0$  and  $l_{ij}^k (y_j^a - y_j^b) \geq 0$

for every  $1 \leq j \leq N$ . Since  $l_{ij}^k$  is always non-negative when  $0 < \epsilon \leq \frac{1}{\|\mathbf{A}_{dag}^k\|_\infty}$ , i.e.,

$$l_{ij}^k = \begin{cases} 1 - \epsilon d_{ij}^k \geq 0, & i = j; \\ \epsilon a_{ij}^k \geq 0, & i \neq j, \end{cases} \quad (50)$$

we can get the first scaling to be an equality requires

$$\begin{cases} x_j^a - x_j^b \geq 0 \\ y_j^a - y_j^b \geq 0 \end{cases} \quad 1 \leq j \leq N. \quad (51)$$

The condition for the second scaling to be equal is

$$|x_j^a - x_j^b| + |y_j^a - y_j^b| = \|\mathbf{X}_{gco}^a - \mathbf{X}_{gco}^b\|_\infty = C \text{ for } \forall j, \quad (52)$$

where  $C \in \mathbb{R}$  is a constant.

Assuming that the two position matrices  $\mathbf{X}_{gco}^a, \mathbf{X}_{gco}^b \in \{\mathbf{X}_{gco} | \sum_{i=1}^N x_i = X_{sum}, \sum_{i=1}^N y_i = Y_{sum}\}$ , we can derive that

$$\begin{aligned} C &= \frac{1}{N} \sum_{j=1}^N |x_j^a - x_j^b| + |y_j^a - y_j^b| \\ &= \frac{1}{N} \sum_{j=1}^N (x_j^a - x_j^b + y_j^a - y_j^b) \\ &= \frac{1}{N} \left( \sum_{j=1}^N x_j^a - \sum_{j=1}^N x_j^b + \sum_{j=1}^N y_j^a - \sum_{j=1}^N y_j^b \right) \\ &= \frac{1}{N} (X_{sum} - X_{sum} + Y_{sum} - Y_{sum}) \\ &= 0. \end{aligned} \quad (53)$$

This indicates that  $x_j^a - x_j^b = 0$  and  $y_j^a - y_j^b = 0$  for every  $1 \leq j \leq N$ . Hence, (47) is an equality if and only if  $\mathbf{X}_{gco}^a = \mathbf{X}_{gco}^b$ , and we have

$$d(g_\theta * \mathbf{X}_{gco}^a, g_\theta * \mathbf{X}_{gco}^b) = d(\mathbf{X}_{gco}^a, \mathbf{X}_{gco}^b) = 0. \quad (54)$$

At this point, we have proved that for  $\forall \mathbf{X}_{gco}^a, \mathbf{X}_{gco}^b \in \{\mathbf{X}_{gco} | \sum_{i=1}^N x_i = X_{sum}, \sum_{i=1}^N y_i = Y_{sum}\}$ , the condition

$$d(g_\theta * \mathbf{X}_{gco}^a, g_\theta * \mathbf{X}_{gco}^b) \leq \alpha d(\mathbf{X}_{gco}^a, \mathbf{X}_{gco}^b) \quad (55)$$

always holds for  $\alpha \in (0, 1)$ . This indicates that the B-GCO is a contraction operation when  $0 < \epsilon \leq \frac{1}{\|\mathbf{A}_{dag}^k\|_\infty}$ , and there exists and only exists one position matrix  $\bar{\mathbf{X}}_{gco} = [\bar{\mathbf{p}}_1, \bar{\mathbf{p}}_{r_2}, \dots, \bar{\mathbf{p}}_N]^\top$  such that

$$\bar{\mathbf{X}}_{gco} = (\mathbf{I}_N - \epsilon \mathbf{L}_{dag}^k) \bar{\mathbf{X}}_{gco} = \lim_{l \rightarrow \infty} (\mathbf{I}_N - \epsilon \mathbf{L}_{dag}^k)^l \mathbf{X}_{gco}, \quad (56)$$

which is also called the *Banach point*.

By eliminating the  $\bar{\mathbf{X}}_d$  on both side, we can derive

$$\mathbf{L}_{dag}^k \bar{\mathbf{X}}_{gco} = \mathbf{L}_{dag}^k [\bar{\mathbf{x}}, \bar{\mathbf{y}}] = \mathbf{0}, \quad (57)$$

where  $\bar{\mathbf{x}}$  and  $\bar{\mathbf{y}}$  are the column vectors in  $\bar{\mathbf{X}}_{gco}$ . This indicates that  $\bar{\mathbf{x}}$  and  $\bar{\mathbf{y}}$  are eigenvectors of  $\mathbf{L}_{dag}^k$  corresponding to the zero eigenvalue. Note that the number of zero eigenvalues of  $\mathbf{L}_{dag}^k$  equals the number of sub-nets in the mDAG, and  $S$  zero eigenvalues  $\lambda_1 = 0, \lambda_2 = 0, \dots, \lambda_S = 0$  correspond to

$S$  orthogonal eigenvectors  $\{\mathbf{u}_1, \mathbf{u}_2, \dots, \mathbf{u}_S\}$ . Thereby, we can represent  $\bar{\mathbf{x}}$  and  $\bar{\mathbf{y}}$  as the linear combinations of  $\mathbf{u}_i$ , i.e.,

$$\begin{cases} \bar{\mathbf{x}}_d = \sum_{i=1}^S \alpha_i \mathbf{u}_i; \\ \bar{\mathbf{y}}_d = \sum_{i=1}^S \beta_i \mathbf{u}_i, \end{cases} \quad (58)$$

where  $\alpha_i, \beta_i \in \mathbb{R}$  are coefficients of the combinations.

When the mDAG is connected, the number of zero eigenvalues of  $\mathbf{L}_{dag}^k$  equals 1. Note that the vector  $\mathbf{1}_N$  must be a eigenvector of  $\mathbf{L}_{dag}^k$  corresponding to the zero eigenvalue, since

$$\mathbf{L}_{dag}^k \mathbf{1}_N = \begin{pmatrix} d_1 - \sum_{j=1}^N a_{1j} \\ d_2 - \sum_{j=1}^N a_{2j} \\ \vdots \\ d_N - \sum_{j=1}^N a_{Nj} \end{pmatrix} = \mathbf{0} = 0 \cdot \mathbf{1}_N. \quad (59)$$

Based on (58), we can get  $\bar{\mathbf{x}} = \alpha_1 \mathbf{1}_N$  and  $\bar{\mathbf{y}} = \beta_1 \mathbf{1}_N$  with  $\alpha_1, \beta_1 \neq 0$ . Since  $\bar{\mathbf{X}}_{gco} \in \{\mathbf{X}_{gco} | \sum_{i=1}^N x_i = X_{sum}, \sum_{i=1}^N y_i = Y_{sum}\}$ , we have

$$\sum_{i=1}^N x_i = \sum_{i=1}^N \alpha_1 \Rightarrow \alpha_1 = \frac{1}{N} X_{sum}, \quad (60)$$

$$\sum_{i=1}^N y_i = \sum_{i=1}^N \beta_1 \Rightarrow \beta_1 = \frac{1}{N} Y_{sum}. \quad (61)$$

Therefore, when the input dilated graph is connected with the feature matrix as  $\mathbf{X}_{in}$ ,  $\bar{\mathbf{X}}_{gco} \equiv [\mathbf{p}_c, \mathbf{p}_c, \dots, \mathbf{p}_c]^\top$  holds. This completes the proof.

## APPENDIX B PROOF OF PROPOSITION 2

The DGCN consists of an input normalization layer,  $Q$  B-GCO layers,  $Q - 1$  nonlinear activation layers, and an output upscale layer. Compared to other operations, the graph convolution within the B-GCO layers takes the most computational complexity. For each B-GCO layer, the GCO applies matrix multiplications for two times in (24). The computational complexity of a single B-GCO layer is the sum of the complexities of matrix multiplications.

For the  $q$ -th B-GCO layer, the first multiplication is the GCO kernel  $g_\theta = \mathbf{I}_{KN} - \epsilon \dot{\mathbf{L}}_{dag}$ , shaped  $KN \times KN$ , multiplying with the feature matrix  $\dot{\mathbf{X}}_{gco}^{q-1}$  with shape of  $KN \times d_{in}^q$ , where  $d_{in}^q$  is the input dimension of the  $q$ -th layer. Notice that the GCO kernel is a block-diagonal matrix calculated by  $\dot{\mathbf{A}}_{dag}$ , and each  $\mathbf{A}_{dag}^k$  has at least  $\frac{1}{2}N^2$  zero elements according to (14). Therefore, the GCO kernel is a sparse matrix, as its ratio of the total number of non-zero elements to the total number of all elements in the matrix is

$$\eta \leq \frac{K \cdot \frac{1}{2}N^2}{KN \cdot KN} = \frac{1}{2K}. \quad (62)$$

Therefore, the computational complexity of the first multiplication is  $\mathcal{O}(\text{nnz}(\mathbf{I}_{KN} - \epsilon \dot{\mathbf{L}}_{dag}) \cdot d_{in}^q)$ .

The number of non-zero elements in the B-GCO kernel is the sum of the numbers of non-zero elements in each branch

with  $A_{dag}^k$ . Let's first analyze the 1-hop branch. The element  $a_{r_i d_j}^1 = 1$  in  $A_{dag}^1$  indicates that the remaining node  $u_{r_i}$  and the destroyed nodes  $u_{d_j}$  established a communication in the original USNET. Assuming that  $N$  nodes are randomly distributed within a  $D \times D$  area, the node degree follows a Poisson distribution with an average degree  $\bar{d}$ . Denote  $p = N_D/N$  as the damage ratio, the number of communication links between the remaining nodes and destroyed nodes is represented as

$$\begin{aligned} \text{nnz}(A_{in, r_i d_j}^1) &= N_R \cdot \bar{d}_R \\ &= (1-p)N \cdot p\bar{d} \\ &= p(1-p)\pi d_{tr}^2 \rho N, \end{aligned} \quad (63)$$

where  $d_{tr}$  is the maximum communication range determined by (2),  $\rho = N/D^2$  is the node density. Therefore, the number of non-zero elements in  $A_{dag}^1$  is  $\text{nnz}(A_{dag}^1) = 2p(1-p)\pi d_{tr}^2 \rho N$  based on (14). For the  $k$ -hop branch, the node degree still follows the Poisson distribution with the mean as  $k\bar{d}$ , hence we have  $\text{nnz}(A_{dag}^k) = k \cdot \text{nnz}(A_{dag}^1)$ . Since  $\text{nnz}(\mathbf{I}_N - \epsilon \mathbf{L}_{dag}^k) = \text{nnz}(A_{dag}^k) + N$ , we have the number of non-zero elements in the B-GCO kernel as

$$\begin{aligned} \text{nnz}(\mathbf{I}_N - \epsilon \mathbf{L}_{dag}) &= \sum_{k=1}^K \text{nnz}(A_{dag}^k) + KN \\ &= \sum_{k=1}^K k \cdot 2p(1-p)\pi d_{tr}^2 \rho N + KN \\ &= p(1-p)\pi d_{tr}^2 \rho K(K-1)N + KN. \end{aligned} \quad (64)$$

The second multiplication in the  $q$ -th layer is the middle matrix with shape  $KN \times d_{in}^q$  multiplying with the weight matrix  $\mathbf{W}^q$ , shaped  $d_{in}^q \times d_{out}^q$ . The computational complexity of the second multiplication is  $\mathcal{O}(KN d_{in}^q d_{out}^q)$ . Therefore, the complexity of the  $q$ -th layer is  $\mathcal{O}(\text{nnz}(\mathbf{I}_{KN} - \epsilon \mathbf{L}_{dag}) \cdot d_{in}^q + KN d_{in}^q d_{out}^q)$ .

The total complexity of DGCN is the sum of the B-GCO layers, i.e.,

$$\begin{aligned} &\mathcal{O}\left(\sum_{q=1}^Q \text{nnz}(\mathbf{I}_{KN} - \epsilon \mathbf{L}_{dag}) \cdot d_{in}^q + KN d_{in}^q d_{out}^q\right) \\ &= \mathcal{O}\left(\sum_{q=1}^Q [p(1-p)\pi d_{tr}^2 \rho K(K-1)N + KN] d_{in}^q + KN d_{in}^q d_{out}^q\right) \\ &= \mathcal{O}\left(KN \sum_{q=1}^Q [p(1-p)\pi d_{tr}^2 \rho (K-1) + 1 + d_{out}^q] d_{in}^q\right). \end{aligned} \quad (65)$$

This completes the proof.

## REFERENCES

- [1] Y. Naidoo, R. Stopforth, and G. Bright, "Development of an uav for search & rescue applications," in *IEEE Africon '11*, 2011, pp. 1–6.
- [2] R. Li and H. Ma, "Research on uav swarm cooperative reconnaissance and combat technology," in *2020 3rd International Conference on Unmanned Systems (ICUS)*, 2020, pp. 996–999.
- [3] H. Jinjiang, W. Husheng, Z. Renjun, M. Rafik, and Z. Xuanwu, "Self-organized search-attack mission planning for uav swarm based on wolf pack hunting behavior," *Journal of Systems Engineering and Electronics*, vol. 32, no. 6, pp. 1463–1476, 2021.
- [4] Z. Han, A. L. Swindlehurst, and K. R. Liu, "Optimization of manet connectivity via smart deployment/movement of unmanned air vehicles," *IEEE Transactions on vehicular technology*, vol. 58, no. 7, pp. 3533–3546, 2009.
- [5] A. Ajorlou, A. Momeni, and A. G. Aghdam, "A class of bounded distributed control strategies for connectivity preservation in multi-agent systems," *IEEE Transactions on Automatic Control*, vol. 55, no. 12, pp. 2828–2833, 2010.
- [6] R. Dutta, L. Sun, and D. Pack, "A decentralized formation and network connectivity tracking controller for multiple unmanned systems," *IEEE Transactions on Control Systems Technology*, vol. 26, no. 6, pp. 2206–2213, 2017.
- [7] S. Lee and M. Younis, "Recovery from multiple simultaneous failures in wireless sensor networks using minimum steiner tree," *Journal of Parallel and Distributed Computing*, vol. 70, no. 5, pp. 525–536, 2010.
- [8] S. Lee, M. Younis, and M. Lee, "Connectivity restoration in a partitioned wireless sensor network with assured fault tolerance," *Ad Hoc Networks*, vol. 24, pp. 1–19, 2015.
- [9] S. Shankar and D. Kundur, "Towards improved connectivity with hybrid uni/omni-directional antennas in wireless sensor networks," in *IEEE INFOCOM Workshops 2008*. IEEE, 2008, pp. 1–4.
- [10] A. A. Abbasi, M. F. Younis, and U. A. Baroudi, "Recovering from a node failure in wireless sensor-actor networks with minimal topology changes," *IEEE Transactions on vehicular technology*, vol. 62, no. 1, pp. 256–271, 2012.
- [11] M. Imran, M. Younis, A. M. Said, and H. Hasbullah, "Volunteer-instigated connectivity restoration algorithm for wireless sensor and actor networks," in *2010 IEEE International Conference on Wireless Communications, Networking and Information Security*. IEEE, 2010, pp. 679–683.
- [12] A. A. Abbasi, M. F. Younis, and U. A. Baroudi, "Recovering from a node failure in wireless sensor-actor networks with minimal topology changes," *IEEE Transactions on vehicular technology*, vol. 62, no. 1, pp. 256–271, 2012.
- [13] Y. Zhang, J. Wang, and G. Hao, "An autonomous connectivity restoration algorithm based on finite state machine for wireless sensor-actor networks," *Sensors*, vol. 18, no. 1, p. 153, 2018.
- [14] A. A. Abbasi, M. F. Younis, and U. A. Baroudi, "Recovering from a node failure in wireless sensor-actor networks with minimal topology changes," *IEEE Transactions on vehicular technology*, vol. 62, no. 1, pp. 256–271, 2012.
- [15] A. A. Abbasi, M. Younis, and K. Akkaya, "Movement-assisted connectivity restoration in wireless sensor and actor networks," *IEEE Transactions on parallel and distributed systems*, vol. 20, no. 9, pp. 1366–1379, 2008.
- [16] M. Younis, S. Lee, and A. A. Abbasi, "A localized algorithm for restoring internode connectivity in networks of moveable sensors," *IEEE Transactions on Computers*, vol. 59, no. 12, pp. 1669–1682, 2010.
- [17] K. Akkaya, I. F. Senturk, and S. Vemulapalli, "Handling large-scale node failures in mobile sensor/robot networks," *Journal of Network and Computer Applications*, vol. 36, no. 1, pp. 195–210, 2013.
- [18] F. Senel and M. Younis, "Optimized connectivity restoration in a partitioned wireless sensor network," in *2011 IEEE global telecommunications conference-GLOBECOM 2011*. IEEE, 2011, pp. 1–5.
- [19] S. Choukhi, I. El Korbi, Y. Ghamri-Doudane, and L. A. Saidane, "Centralized connectivity restoration in multichannel wireless sensor networks," *Journal of Network and Computer Applications*, vol. 83, pp. 111–123, 2017.
- [20] Y. Zhang, Z. Zhang, and B. Zhang, "A novel hybrid optimization scheme on connectivity restoration processes for large scale industrial wireless sensor and actuator networks," *Processes*, vol. 7, no. 12, p. 939, 2019.
- [21] Z. Mi, Y. Yang, and G. Liu, "Hero: A hybrid connectivity restoration framework for mobile multi-agent networks," in *2011 IEEE International Conference on Robotics and Automation*, 2011, pp. 1702–1707.
- [22] M. Chen, H. Wang, C.-Y. Chang, and X. Wei, "Sidr: A swarm intelligence-based damage-resilient mechanism for uav swarm networks," *IEEE Access*, vol. 8, pp. 77 089–77 105, 2020.
- [23] Z. Mou, F. Gao, J. Liu, and Q. Wu, "Resilient uav swarm communications with graph convolutional neural network," *IEEE Journal on Selected Areas in Communications*, vol. 40, no. 1, pp. 393–411, 2022.
- [24] H. Lin, L. Ding, S. Chen, F. Yang, and L. Qian, "Multi-hop diffused graph convolution for resilient uav swarm networks," in *2024 IEEE International Symposium on Broadband Multimedia Systems and Broadcasting (BMSB)*. IEEE, 2024, pp. 1–6.
- [25] T. N. Kipf and M. Welling, "Semi-supervised classification with graph convolutional networks," *arXiv preprint arXiv:1609.02907*, 2016.

- [26] A. Phadke and F. A. Medrano, "Towards resilient uav swarms—a breakdown of resiliency requirements in uav swarms," *Drones*, vol. 6, no. 11, p. 340, 2022.
- [27] M. Younis, I. F. Senturk, K. Akkaya, S. Lee, and F. Senel, "Topology management techniques for tolerating node failures in wireless sensor networks: A survey," *Computer networks*, vol. 58, pp. 254–283, 2014.
- [28] B. Mohar, Y. Alavi, G. Chartrand, and O. Oellermann, "The laplacian spectrum of graphs," *Graph theory, combinatorics, and applications*, vol. 2, no. 871-898, p. 12, 1991.
- [29] U. Von Luxburg, "A tutorial on spectral clustering," *Statistics and computing*, vol. 17, pp. 395–416, 2007.
- [30] N. Srivastava, G. Hinton, A. Krizhevsky, I. Sutskever, and R. Salakhutdinov, "Dropout: a simple way to prevent neural networks from overfitting," *The journal of machine learning research*, vol. 15, no. 1, pp. 1929–1958, 2014.
- [31] M. Oehlers and B. Fabian, "Graph metrics for network robustness—a survey," *Mathematics*, vol. 9, no. 8, p. 895, 2021.
- [32] S. Brody, U. Alon, and E. Yahav, "How attentive are graph attention networks?" *arXiv preprint arXiv:2105.14491*, 2021.